Editors' Suggestion

Bose polaron and the Efimov effect: A Gaussian-state approach

Arthur Christianen,[1,2,*] J. Ignacio Cirac,[1,2] and Richard Schmidt[1,2,3,†]

[1]*Max-Planck-Institut für Quantenoptik, Hans-Kopfermann-Straße 1, D-85748 Garching, Germany*

[2]*Munich Center for Quantum Science and Technology, Schellingstraße 4, D-80799 Munich, Germany*

[3]*Department of Physics and Astronomy, Aarhus University, DK-8000 Aarhus C, Denmark*

(Received 27 October 2021; revised 16 February 2022; accepted 4 April 2022; published 4 May 2022)

Since the Efimov effect was introduced, a detailed theoretical understanding of Efimov physics has been developed in the few-body context. However, it has proven challenging to describe the role Efimov correlations play in many-body systems such as quenched or collapsing Bose-Einstein condensates (BECs). To study the impact the Efimov effect has in such scenarios, we consider a light impurity immersed in a weakly interacting BEC, forming a Bose polaron. In this case, correlations are localized around the impurity, making it more feasible to develop a theoretical description. Specifically, we employ a variational Gaussian state *Ansatz* in the reference frame of the impurity, capable of capturing both the Efimov effect and the formation of a polaron cloud consisting of a macroscopic number of particles. We find that the Efimov effect entails cooperative binding of bosons to the impurity, leading to the formation of large clusters. These many-particle Efimov states exist for a wide range of scattering lengths, with energies significantly below the polaron energy. As a result, the polaron is not the ground state, but rendered a metastable excited state which can decay into these clusters. While this decay is slow for small interaction strengths, it becomes more prominent as the attraction increases, up to a point where the polaron becomes completely unstable. We show that the critical scattering length where this happens can be interpreted as a many-body shifted Efimov resonance, where the scattering of two excitations of the bath with the polaron can lead to polaron-cloud assisted bound-state formation. Compared to the few-body case, the resonance is shifted to weaker attraction due to the participation of the polaron cloud in the cooperative binding process. This represents an intriguing example of chemistry in a quantum medium [A. Christianen *et al.*, Phys. Rev. Lett. **128**, 183401 (2022)], where many-body effects lead to a shift in the resonances of the chemical recombination, which can be directly probed in state-of-the-art experiments.

DOI: 10.1103/PhysRevA.105.053302

I. INTRODUCTION

To describe the properties of a many-body system, an accurate understanding of the relevant interactions and correlations between its microscopic constituents is crucial. However, even when the few-body physics is understood, extracting the emergent properties of the system as a whole is not a simple task [1]. A good example is the Efimov effect [2,3]. This fascinating few-body phenomenon was predicted by Efimov in the context of nuclear physics. Efimov showed that there exists an infinite series of three-body bound states close to the unitarity point of a Feshbach resonance with binding energies obeying a geometric scaling law. The experimental demonstration of this effect took more than 30 years, with first observations in cold atomic gases [4] and later in helium [5]. Driven by further experiments, by now a good theoretical understanding of the few-body physics has been developed [3]. However, the task to understand the effect Efimov-like correlations have on quantum many-body systems has proven to be challenging and has recently attracted particular interest in the context of quenched or collapsing Bose-Einstein condensates (BECs), especially at unitary interactions [6–14]. In such systems the rapid buildup of three-body and higher-order correlations renders the description a challenge whose solution remains elusive.

Here we approach this challenge by developing an understanding of the effect Efimov-like correlations have in a many-body setting by considering the simpler problem of a mobile impurity immersed in a weakly interacting BEC. Such a quantum impurity is dressed by fluctuations in its environment, leading to the formation of a Bose polaron. Importantly, this problem exhibits the heteronuclear instead of the homonuclear Efimov effect and the relevant three-body processes always involve the impurity. As a result, the most important three-body correlations are localized around the impurity, making the theoretical description more feasible. In particular, this allows the use of variational approaches [15–17], which is much more difficult when higher-order correlations throughout a whole BEC have to be accounted for. Also experimentally, probing the Bose polaron can

*arthur.christianen@mpq.mpg.de
†richard.schmidt@mpq.mpg.de

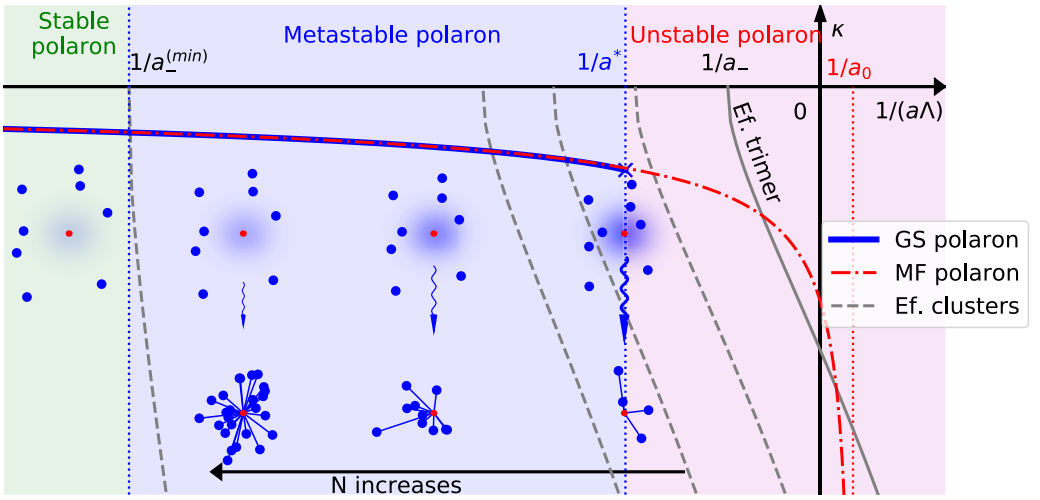

FIG. 1. Illustration of the main results of this work. Here we show the wave number $\kappa = -\frac{\sqrt{M|E|}}{\Lambda}$ of the polaron found using Gaussian states (blue solid line) and mean-field theory (red dash-dotted line) as a function of the inverse scattering length $1/a\Lambda$. In gray the wave number of the Efimov trimer (solid line) and larger Efimov clusters (dashed lines) is shown. Note that the dashed lines are only representative and not all possible Efimov clusters are displayed. For small scattering lengths (green area), the polaron is the ground state of the system and a stable quasiparticle. For $|a| > |a_-^{(\mathrm{min})}|$, the smallest scattering length at which an Efimov cluster can be formed, the polaron turns into a metastable excited state, which can decay into the large Efimov clusters via many-body scattering processes. These scattering processes become more likely as the absolute value of the scattering length increases. When a critical scattering length a^* is reached, the polaron ceases to exist as a well-defined quasiparticle. At this point scattering of the polaron with one or two more bath particles can lead to the rapid decay into an Efimov cluster. In contrast, in mean-field theory, the polaron remains stable up to a positive scattering length a_0, at which an infinite number of particles piles up in two-body bound states formed with the impurity.

give new insight, due to the available techniques such as radio-frequency (rf) spectroscopy [18–20] or Ramsey interferometry [21].

The concept of the Bose polaron as an impurity immersed in a bath of bosonic excitations was introduced by Landau [22] to describe an electron dressed by phonons in a solid. A model that is commonly used in condensed matter to describe this scenario is the Fröhlich model [23]. However, the Fröhlich Hamiltonian does not contain all necessary terms to describe bound-state formation, while this is crucial in the formation of the cold-atom Bose polaron [24]. Therefore, an extension of the Fröhlich model is required. The situation is further complicated by the fact that the description of the wave function needs to include the relevant interboson correlations, rendering the Bose polaron problem in the cold-atom context a challenge. Whereas the Fermi polaron problem can be understood with relatively simple theoretical models [25–27], various descriptions of the strong-coupling Bose polaron have yielded widely varying results [15–17,28–31]. In Refs. [15,17] variational *Ansätze* based on a small number of excitations were used and a smooth crossover between the polaron and an Efimov state was predicted, with energies in agreement with quantum Monte Carlo calculations in Ref. [28]. However, when using a coherent state variational *Ansatz* which is capable of truly describing a mesoscopic deformation of the BEC instead of only excitations on top of the homogeneous BEC, one finds that the polaron becomes unstable due to an infinite number of excitations piling up on the impurity [16]. This instability is prevented by explicitly taking into account interboson repulsion [30–35], but still the polaron cloud will contain a large number of particles. What the coherent state approach clearly lacks, however, are interboson correlations, meaning the Efimov effect cannot be captured. Also, while renormalization-group theory [29] predicts the polaron to be unstable already for negative scattering lengths, no clear connection to Efimov physics is evident.

In this work we systematically extend the coherent state *Ansatz* by fully including two-body interboson correlations and three-body correlations involving the impurity. To achieve this, we use Gaussian states [36] in the reference frame of the impurity. As a result, we can describe both the many-body physics of the creation of a macroscopic polaron cloud and the few-body physics of the Efimov effect. In particular, we study how these two phenomena affect each other. We focus on the case of light impurities where the impurity can more efficiently mediate interactions between the bosons and the Efimov effect is thus most prominent [3,37–41].

One of our key results, illustrated in Fig. 1, is that the polaron is no longer the ground state of the extended Fröhlich Hamiltonian when three-body correlations are taken into account. This finding is a result of large Efimov clusters that emerge deeply in the energy spectrum. However, the polaron remains a metastable excited state up to a critical scattering length a^*, at which an energy barrier protecting the polaron from decaying into Efimov clusters disappears. This critical scattering length can be interpreted as a many-body shifted Efimov resonance.

Our results find an intuitive explanation when first considering the question of how the heteronuclear Efimov effect extends to the case of more than three particles. For the homonuclear case this extension to larger particle numbers is well understood [3,42] and four- and five-particle Efimov clusters have been experimentally observed [43,44]. In this case larger and larger clusters are more and more tightly

bound. This can be understood from simple dimensional arguments [3]. When the atoms have pairwise interactions the attractive interaction energy grows with N^2, whereas the kinetic energy, counteracting bound-state formation, only grows with N. The situation is not as clear in the heteronuclear case. When the bosons only interact attractively with the impurity, but do not interact or interact only repulsively with each other, also the interaction energy scales with N. Thus, a nontrivial competition between the kinetic and potential energy arises and the simple dimensional argument breaks down. As a result, there is no general picture for the existence of clusters with increasing size in the heteronuclear case.

Here we assume weakly interacting bosons and use a single-channel model to describe the interactions with the impurity. We show that in this scenario, similar to the homonuclear case, clusters of increasing particle number become more and more tightly bound. We will refer to this effect as cooperative binding. This term originates from chemistry, where it refers to particles cooperating with each other to lead to ever stronger binding, such as in the famous example of oxygen binding to hemoglobin.

Strikingly, we find that the cooperative binding effect has a profound impact on the stability of Bose polarons. This is also illustrated in Fig. 1, where we schematically plot the wave number of the polaron state found from Gaussian (blue solid line) and coherent states (red dash-dotted line) as a function of the dimensionless scattering length. The result from coherent states is referred to as mean-field theory. The gray solid line indicates the position of the lowest three-body Efimov state in vacuum, appearing at the three-atom scattering threshold at a_-. The gray dashed lines indicate the lowest Efimov clusters of increasing particle number, which shift to the left as a function of particle number. Using simple arguments, we prove that there is a minimum scattering length $a_-^{(\mathrm{min})}$ needed to form any Efimov cluster, which is indicated as the boundary of the green shaded area in Fig. 1.

The background color of the figure indicates the stability of the polaron. In the green area, no Efimov cluster can be formed, meaning that the polaron is the ground state of the extended Fröhlich Hamiltonian. When crossing $a_-^{(\mathrm{min})}$ into the blue area, the polaron is no longer the absolute ground state, but becomes a metastable excited state. For scattering lengths $|a| < |a^*|$, the decay of the polaron into Efimov clusters, indicated by wiggly vertical arrows, is extremely slow and requires the simultaneous scattering of a large number of bosons on the polaron. However, as the magnitude of the scattering length increases, the number of particles in the polaron cloud increases and the number of particles needed to form a bound state decreases. As a result, the decay processes will become more and more pronounced. When a^* is crossed into the red area, already scattering of only one or two additional bosons is sufficient to cause the breakdown of the polaron into an Efimov cluster. Since these decay processes are included in our Gaussian state *Ansatz*, the local energy minimum of the polaron on our variational manifold disappears, meaning the polaron is no longer a metastable quasiparticle. Since the classical field of the background BEC mixes the different particle number clusters, we find a cascade of the wave function into ever larger Efimov clusters.

One remarkable outcome of our study is that $|a^*|$ is smaller than $|a_-|$. This is caused by the fact that the polaron can decay immediately into larger clusters than the Efimov trimer, requiring smaller scattering lengths due to the cooperative binding. In experiments, the formation of these large Efimov clusters will cause rapid chemical recombination into deeply bound states not included in our model. Furthermore, the shift of the Efimov resonance means that the experimentally observed resonant recombination signal will be modified by the presence of the BEC. This provides a fascinating example of how chemistry is modified in a quantum medium and how polaron cloud formation can enhance chemical reactivity [45].

The structure of the paper is as follows. After introducing our theoretical methods in Sec. II, we prove in Sec. III that our Gaussian state *Ansatz* incorporates Efimov physics. Moreover, we present evidence for the cooperative binding effect extending to large particle numbers and we elucidate the origin of this effect. We demonstrate that many-body Efimov clusters form the ground state of the Hamiltonian. Then, in Sec. IV, we use the Gaussian state *Ansatz* to calculate the energy of the polaron as a function of scattering length and density and we demonstrate its abrupt instability. In Sec. V we discuss in detail the relation of our work to other theoretical methods and how our results can be probed experimentally. We conclude in Sec. VI with an outlook on future work.

II. THEORETICAL METHODS

A. Hamiltonian

To describe the impurity immersed in a three-dimensional, homogeneous, weakly interacting BEC at zero temperature, we use the extended Fröhlich model introduced in Ref. [24], described by the Hamiltonian

$$\hat{\mathcal{H}}_0 = \int d\boldsymbol{k}\frac{\boldsymbol{k}^2}{2m}\hat{a}_{\boldsymbol{k}}^\dagger\hat{a}_{\boldsymbol{k}} + \frac{\hat{\boldsymbol{P}}^2}{2M} + g\int d\boldsymbol{r}\,\delta(\boldsymbol{r}-\hat{\boldsymbol{R}})\hat{a}_{\boldsymbol{r}}^\dagger\hat{a}_{\boldsymbol{r}} + \frac{g_B}{2}\iint d\boldsymbol{r}\,d\boldsymbol{r}'\delta(\boldsymbol{r}-\boldsymbol{r}')\hat{a}_{\boldsymbol{r}'}^\dagger\hat{a}_{\boldsymbol{r}}^\dagger\hat{a}_{\boldsymbol{r}'}\hat{a}_{\boldsymbol{r}}. \quad (1)$$

Here we treat the impurity with mass M in first quantization with position and momentum operators $\hat{\boldsymbol{R}}$ and $\hat{\boldsymbol{P}}$. The bosons of mass m are described using second quantization, where operators $\hat{a}_{\boldsymbol{k}}^\dagger$ and $\hat{a}_{\boldsymbol{k}}$ create and annihilate bosons of momentum $\boldsymbol{k}$, respectively. The bosons interact via a contact interaction with scattering length a_B determined by a coupling strength g_B. The boson-impurity interaction is modeled using a regularized contact interaction of strength g with corresponding scattering length a. In Eq. (1), $\int d\boldsymbol{k}$ is shorthand for $\int \frac{d^3k}{(2\pi)^3}$. We have used a single-channel model to describe the interactions, which provides a good description of the interactions in the vicinity of a broad Feshbach resonance.

We model the bosons within the Bogoliubov approximation and introduce the corresponding quasiparticle operators $\hat{b}_{\boldsymbol{k}}^\dagger$ and $\hat{b}_{\boldsymbol{k}}$. The validity of this approximation will be discussed in detail in the following sections. After the Bogoliubov rotation, we apply the unitary Lee-Low-Pines transformation [46] $\hat{U}_{\mathrm{LLP}}$ to translate into the frame of the impurity,

$$\hat{U}_{\mathrm{LLP}} = \exp\left(-i\hat{\boldsymbol{R}}\int d\boldsymbol{k}\,\boldsymbol{k}\,\hat{b}_{\boldsymbol{k}}^\dagger\hat{b}_{\boldsymbol{k}}\right). \quad (2)$$

Crucially, this transformation reduces the number of degrees of freedom by eliminating the impurity operators from the problem. The transformed Hamiltonian $\hat{\mathcal{H}} = \hat{U}^\dagger_{\mathrm{LLP}}\hat{\mathcal{H}}_0\hat{U}_{\mathrm{LLP}}$ reads

$$\begin{aligned}\hat{\mathcal{H}} = &\int d\boldsymbol{k}\,\omega_k \hat{b}^\dagger_{\boldsymbol{k}}\hat{b}_{\boldsymbol{k}} + \frac{(\boldsymbol{P} - \int d\boldsymbol{k}\,\boldsymbol{k}\,\hat{b}^\dagger_{\boldsymbol{k}}\hat{b}_{\boldsymbol{k}})^2}{2M} \\ &+ gn_0 + g\sqrt{n_0}\int d\boldsymbol{k}\,W_k(\hat{b}^\dagger_{\boldsymbol{k}} + \hat{b}_{-\boldsymbol{k}}) \\ &+ g\iint d\boldsymbol{k}\,d\boldsymbol{k}'\left(V^{(1)}_{k,k'}\hat{b}^\dagger_{\boldsymbol{k}}\hat{b}_{\boldsymbol{k}'} + \frac{V^{(2)}_{k,k'}}{2}(\hat{b}^\dagger_{\boldsymbol{k}}\hat{b}^\dagger_{\boldsymbol{k}'} + \hat{b}_{-\boldsymbol{k}}\hat{b}_{-\boldsymbol{k}'})\right).\end{aligned} \tag{3}$$

Since the impurity momentum operator $\hat{\boldsymbol{P}}$ now commutes with the Hamiltonian, it has been replaced by a vector $\boldsymbol{P}$, which is the total conserved momentum of the system. We set $\boldsymbol{P} = 0$. In Eq. (3), n_0 is the density of the BEC and definitions of the variables W_k, $V^{(1)}_{k,k'}$, $V^{(2)}_{k,k'}$, and ω_k are given in Appendix A.

To regularize the boson-impurity contact interaction g, we introduce a UV cutoff Λ on all momentum integrals. The solution of the Lippmann-Schwinger equation then yields the renormalization condition

$$g^{-1} = \frac{\mu_r}{2\pi a} - \frac{\mu_r\Lambda}{\pi^2}, \tag{4}$$

where $\mu_r = \frac{mM}{m+M}$ is the reduced mass. The value of Λ^{-1} is related to the effective range of the potential [47] and is proportional to the van der Waals length l_{vdW}. It therefore determines the so-called three-body parameter that sets the position of the first Efimov resonance at negative scattering length a_-. The value of Λ in our model is chosen so that the obtained value of a_- matches the experimental value of the system of interest.

To reduce computational complexity in solving Eq. (3), we make use of the spherical symmetry of the problem and transform from plane-wave modes to spherical waves:

$$\hat{b}^\dagger_{\boldsymbol{k}} = (2\pi)^{3/2}k^{-1}\sum_{lm} i^l Y^*_{lm}(\boldsymbol{\Omega}_k)\hat{b}^\dagger_{klm}. \tag{5}$$

After normal ordering the remaining quartic term in Eq. (3), giving rise to a modified dispersion of the quasiparticles $\omega_k + \frac{k^2}{2M}$, the Hamiltonian takes the form

$$\begin{aligned}\hat{\mathcal{H}} = &\sum_{lm}\int_k\left(\omega_k + \frac{k^2}{2M}\right)\hat{b}^\dagger_{klm}\hat{b}_{klm} \\ &+ \iint d\boldsymbol{k_1}d\boldsymbol{k_2}\frac{\boldsymbol{k}_1\cdot\boldsymbol{k}_2}{2M}\hat{b}^\dagger_{\boldsymbol{k}_1}\hat{b}^\dagger_{\boldsymbol{k}_2}\hat{b}_{\boldsymbol{k}_1}\hat{b}_{\boldsymbol{k}_2} \\ &+ gn_0 + \frac{g\sqrt{n_0}}{\pi\sqrt{2}}\int_k k\,W_k(\hat{b}^\dagger_{k00} + \hat{b}_{k00}) \\ &+ \frac{g}{2\pi^2}\int_{k_1}\int_{k_2}\left(k_1k_2V^{(1)}_{k_1,k_2}\hat{b}^\dagger_{k_100}\hat{b}_{k_200}\right. \\ &\left.+ \frac{V^{(2)}_{k_1,k_2}}{2}(\hat{b}^\dagger_{k_100}\hat{b}^\dagger_{k_200} + \hat{b}_{k_100}\hat{b}_{k_200})\right).\end{aligned} \tag{6}$$

Here we have defined $\int_k \equiv \int_0^\Lambda dk$. The regularized contact interaction only acts on the s-wave component of the wave function.

The second term in Eq. (6) is written without the transformation to spherical waves. Since the full expression after the transformation is very lengthy, we give its explicit form in Appendix B. This term plays a critical role in describing the Efimov effect and we will denote it by $\hat{\mathcal{H}}_{\mathrm{QLLP}}$. Indeed, $\hat{\mathcal{H}}_{\mathrm{QLLP}}$ is the only quartic term of the Hamiltonian. It is thus solely responsible for describing the effective interboson interactions mediated by the impurity. Due to the vector product $\boldsymbol{k}_1\cdot\boldsymbol{k}_2$, it contains the information about the relative motion of the bosons, allowing them to distribute kinetic energy more efficiently. In the spherical representation this manifests as a coupling between consecutive angular momentum terms.

Note that even though we have set $\boldsymbol{P} = 0$, this does not mean that the impurity is stationary. Indeed, despite $\langle\hat{\boldsymbol{P}}\rangle = 0$, $\langle\hat{\boldsymbol{P}}^2\rangle$ is nonzero in the laboratory frame, and it is these fluctuations in the impurity momentum (and its resulting kinetic energy) that will be crucially important our findings.

B. Gaussian states

Throughout this work we use a variational method based on a Gaussian state *Ansatz*. The use of Gaussian states to describe the Bose polaron was previously suggested in Ref. [48] in a perturbative approach. However, the simpler Fröhlich Hamiltonian was considered, which does not allow the description of bound-state physics and thus Efimov physics. Here we use Gaussian states nonperturbatively, applying the formalism outlined in the review by Shi *et al.* [36]. Note that since we use the Lee-Low-Pines transformation, the impurity degrees of freedom are entangled with the bosons, effectively giving a beyond-Gaussian *Ansatz* in the laboratory frame. In the following, we use notation most similar to the presentation in Ref. [49].

The variational *Ansatz* in the impurity frame has the form

$$\begin{aligned}|\psi\rangle = &\exp\left(\sum_{lm}\int_k \hat{\Psi}^\dagger_{klm}\sigma^z\Phi_{klm}\right) \\ &\times\exp\left(\frac{i}{2}\sum_{l,l',m,m'}\int_k\int_{k'}\hat{\Psi}^\dagger_{klm}\Xi_{klm,k'l'm'}\hat{\Psi}_{k'l'm'}\right)|\mathrm{BEC}\rangle,\end{aligned} \tag{7}$$

In this equation $\hat{\Psi}_{klm} = (\hat{b}_{klm}, \hat{b}^\dagger_{klm})^T$ is the Nambu vector containing the bosonic creation and annihilation operators, σ^z is the Pauli z matrix, $\Phi_{klm} = \langle\hat{\Psi}_{klm}\rangle = (\phi_{klm}, \phi^*_{klm})^T$ is the coherent displacement vector, and Ξ is the Hermitian correlation matrix. Our *Ansatz* acts on $|\mathrm{BEC}\rangle$, which is the state of the background BEC. Note that there is no need to further specify the state of the impurity since, in the transformed frame, the impurity is stationary at the center of the frame. When Ξ is set to zero, one is left with the coherent state *Ansatz* from Ref. [16], which we will refer to as mean-field theory.

The *Ansatz* (7) is treated fully variationally with the coherent displacement $\boldsymbol{\Phi}$ and the covariance matrix $\Gamma_{klm,k'l'm'} = \langle\{\delta\hat{\Psi}_{klm}, \delta\hat{\Psi}^\dagger_{k'lm'}\}\rangle$ of the fluctuation field $\delta\hat{\Psi}_{klm} = \hat{\Psi}_{klm} - \Phi_{klm}$ as the variational parameters. The covariance matrix Γ is related to Ξ via the symplectic matrix $S = \exp(i\Sigma^z\Xi)$ as $\Gamma = SS^\dagger$, where $\Sigma^z = \sigma^z\delta(k-k')\delta_{l,l'}\delta_{m,m'}$. Two complementary algorithms are employed to optimize the variational

parameters and to find the energy minima on our variational manifold. The first is imaginary-time evolution and the second iterated Bogoliubov theory. Although both algorithms are in principle equivalent [50], dependent on the situation, either one may be computationally more efficient.

The equations of motion (EOMs) for the imaginary-time evolution are given by [36]

$$\partial_\tau \Phi = -\Gamma(\eta, \eta^*)^T, \tag{8}$$

$$\partial_\tau \Gamma = \Sigma^z \mathscr{H} \Sigma^z - \Gamma \mathscr{H} \Gamma. \tag{9}$$

Here we define

$$E = \langle \mathrm{GS}|\hat{\mathcal{H}}|\mathrm{GS}\rangle, \tag{10}$$

$$\eta_{klm} = \frac{\partial E}{\partial \phi^*_{klm}}, \tag{11}$$

$$\mathscr{H}_{klm,k'l',m'} = \frac{2\partial E}{\partial \Gamma^*_{klm,k'l'm'}} \tag{12}$$

and calculate the expectation value of the Hamiltonian using Wick's theorem. The EOMs are then solved using standard numerical algorithms.

Within iterated Bogoliubov theory, one sequentially solves $\eta = 0$ for ϕ in order to update the displacement. Following that, one diagonalizes $\mathscr{H}$ using a symplectic matrix S, which updates $\Gamma = SS^\dagger$. Performing a single iteration of this algorithm is equivalent to solving the Gross-Pitaevskii equation (solving for ϕ) and calculating the equivalent of the Lee-Huang-Yang correction (diagonalizing $\mathscr{H}$) [49]. Repeated iteration results in predictions beyond the theory of Lee-Huang-Yang corrections. We note that the iterated Bogoliubov theory is especially efficient compared to imaginary-time evolution in the case of very slow dynamics and when η is linear in ϕ.

As we will discuss in the following, for some of our calculations we will fix the expectation value of the particle number during the optimization. For the imaginary-time evolution this is achieved by adding a chemical potential term $\mu_N \hat{N}$ to the Hamiltonian, where $\hat{N}$ is the particle number operator. Using the relation [51]

$$\mu_N = \frac{\langle \hat{N}\hat{\mathcal{H}}\rangle - \langle \hat{N}\rangle\langle \hat{\mathcal{H}}\rangle}{\langle \hat{N}^2\rangle - \langle \hat{N}\rangle^2}, \tag{13}$$

the chemical potential μ_N is dynamically adjusted to keep the particle number fixed during the time evolution.

III. EFIMOV CLUSTERS AND COOPERATIVE BINDING

Cooperative binding, which describes particles helping each other to bind to an object, is an important aspect of the Efimov effect. This is immediately apparent from the fact that three-particle Efimov states can be formed even when no dimers can be formed. In this section we demonstrate that this cooperative binding can in fact persist for an arbitrary number of particles. In terms of the illustration in Fig. 1, this means that the gray dashed lines move farther and farther to the left as the particle number N increases.

A. The two- and three-body problem

1. *Variational* Ansätze

Before studying the formation of large clusters, it is instructive to first consider the two- and three-body problem (i.e., the case of one or two bosons plus the impurity). In order to restrict ourselves to the case of fixed particle number, we set the background density n_0 in Eq. (6) to zero. Moreover, we consider noninteracting bosons ($a_B = 0$), yielding the Hamiltonian

$$\hat{\mathcal{H}} = \sum_{lm}\int_k \frac{k^2}{2\mu_r}\hat{b}^\dagger_{klm}\hat{b}_{klm} + \hat{\mathcal{H}}_{\mathrm{QLLP}} + \frac{g}{2\pi^2}\int_{k_1}\int_{k_2} k_1 k_2 \hat{b}^\dagger_{k_1 00}\hat{b}_{k_2 00}. \tag{14}$$

For the two- and three-body problem, we use the exact variational *Ansätze*

$$|\psi_{2b}\rangle = \int_k \beta_k \hat{b}^\dagger_{k00}|0\rangle, \tag{15}$$

$$|\psi_{3b}\rangle = \frac{1}{\sqrt{2}}\sum_{lm}\int_{k_1}\int_{k_2}(-1)^m \alpha_{k_1 k_2 l}\hat{b}^\dagger_{k_1 lm}\hat{b}^\dagger_{k_2 l-m}|0\rangle, \tag{16}$$

where angular momentum conservation has been taken into account and the total angular momentum has been set to zero. In the two-body problem [Eq. (15)], this directly implies that the single boson always has angular momentum zero, whereas in the three-body problem [Eq. (16)], the two bosons always have opposite angular momenta in the frame of the impurity. Moreover, the wave function α depends only on m with the sign $(-1)^m$, reflecting spherical symmetry.

In the few-body case the eigenenergies, and in particular the ground-state energy, can be readily obtained by the diagonalization of the real-time EOMs instead of using imaginary-time evolution. It turns out that, despite the complex form of $\hat{\mathcal{H}}_{\mathrm{QLLP}}$, the real-time EOMs are relatively simple when the symmetries are implemented. One finds

$$i\partial_t \beta_k = \frac{k^2\beta_k}{2\mu_r} + \frac{gk}{2\pi^2}\int_{k'} k'\beta'_k, \tag{17}$$

$$i\partial_t \alpha_{k_1 k_2 l} = \alpha_{k_1 k_2 l}\frac{k_1^2 + k_2^2}{2\mu_r} + \frac{g\delta_{l,0}}{2\pi^2}\int_k k(k_2\alpha_{k_1 k 0} + k_1\alpha_{k k_2 0}) - \frac{k_1 k_2}{M(2l+1)}[(l+1)\alpha_{k_1 k_2 (l+1)} + l\alpha_{k_1 k_2 (l-1)}], \tag{18}$$

which can be diagonalized using standard numerical techniques.

2. *Noninteracting problem*

First, we consider the noninteracting problem ($g = 0$). In this case the momentum of each particle is a good quantum number. As a result, the two-body problem is trivial. Since the total momentum is fixed to zero, the impurity and the boson will always have opposite momenta. This directly yields the energy $\frac{k^2}{2\mu_r}$. The $\hat{\mathcal{H}}_{\mathrm{QLLP}}$ term vanishes in the two-body problem and thus plays no role.

In contrast, for the three-body problem, the EOMs *in the impurity frame* [Eq. (18)] are nontrivial, since the $\hat{\mathcal{H}}_{\mathrm{QLLP}}$

term couples the different angular momentum modes. This coupling is indeed crucial since the lowest energy for total momentum $\boldsymbol{P} = 0$ and fixed momenta of the two bosons k_1 and k_2 occurs when the two particles move in opposite directions. This means that the direction of motion of the bosons in the impurity frame needs to be correlated.

To proceed in this case, one may note that the noninteracting EOMs of the three-body problem can be mapped to the problem of two coupled harmonic oscillators. This in turn can be solved exactly using a Bogoliubov rotation. One obtains the energy $\frac{k_1^2+k_2^2}{2m} + \frac{(k_1-k_2)^2}{2M}$, corresponding to an impurity momentum of $k_1 - k_2$, which shows that the bosons indeed move in opposite directions. In the corresponding wave function every angular momentum mode is equally populated. This implies that an infinite number of modes is required to solve the usually trivial noninteracting problem in this framework. Fortunately, for finite $g < 0$, as considered below, lower angular momentum modes are favored since only the zeroth angular momentum mode has an (attractive) coupling with the impurity. In the case of bound-state formation, this means that in practice convergence can be achieved with a small number of angular modes.

3. Including interactions

Next we consider the case of a finite negative g. In the two-body problem, a bound state is formed for positive scattering lengths which vanishes into the scattering continuum at unitarity, where $a \to \infty$. However, for three particles, due to the Efimov effect, a bound state can already be formed for finite negative scattering lengths [2,3]. Already for three particles the Efimov effect can therefore be regarded as an instance of cooperative binding, which is driven by the $\hat{\mathcal{H}}_{\mathrm{QLLP}}$ term of the Hamiltonian. Indeed, when $\hat{\mathcal{H}}_{\mathrm{QLLP}}$ is not included [i.e., omitting the second line of Eq. (18)], the EOMs become separable and the EOMs of the two-body problem are retrieved. This demonstrates that the $\hat{\mathcal{H}}_{\mathrm{QLLP}}$ term must be crucial for the Efimov effect. Since this term originates from the kinetic energy of the impurity, it becomes evident that reducing the kinetic energy of the impurity is the driving force of the Efimov effect.

The full three-body problem can be solved numerically using sparse matrix diagonalization employing either linear or, more efficiently, logarithmic grids in k. In this way, the ground and low-lying excited Efimov states can be studied. While the method can be generalized relatively easily to arbitrary interaction potentials, including boson-boson interactions in this framework leads to involved expressions for the relevant matrix elements and removes the sparsity of the matrices representing the equations of motion, greatly increasing numerical complexity.

Focusing on the ground state, we calculate the Efimov scattering length a_- following from our model for ^{6}Li atoms interacting with several types of bosons. The results are shown in Table I. We find that a_- is smallest for light impurities, meaning that the cooperative binding is the strongest in that case. This can easily be understood from the underlying mechanism: the reduction of the kinetic energy of the impurity compared to the interaction energy. Because the kinetic energy of the impurity for a given momentum is larger for light than for heavy impurities, the reduction of this energy can have a larger impact. This is directly reflected in the $\hat{\mathcal{H}}_{\mathrm{QLLP}}$ term of the Hamiltonian, which scales inversely with the mass of the impurity. As a result, a_- quickly grows as the mass ratio m/M decreases. Hence observing Efimov physics experimentally can most easily be achieved by immersing a light impurity in a bath of heavy bosons. Motivated by this fact, for most of the predictions in this work we will focus, as an example, on the mass ratio of the experimentally available system of a ^{6}Li impurity immersed in a BEC of ^{133}Cs atoms [39,40].

TABLE I. Scattering lengths a_- where the lowest-energy three-body Efimov states cross the scattering threshold for ^{6}Li interacting with different species of bosons, using a regularized contact interaction in units of the three-body parameter Λ.

Species	$a_-\Lambda$
^{168}Er	−5.20
^{133}Cs	−5.69
^{87}Rb	−6.91
^{41}K	−11.1
^{23}Na	−19.0
^{7}Li	−135

B. Many-body Efimov effect

We now have to demonstrate that the cooperative binding effect driving the Efimov effect also persists for larger particle numbers. To this end, we need to show that the binding energy per boson $E_{\mathrm{bind}}/N = |E/N|$ increases monotonically with the number N of bound particles.

In order to study N-body bound states, the methods used in the preceding section need to be extended to higher particle numbers. However, pursuing the same route of exactly solving the N-body problem rapidly becomes computationally intractable. Instead, we adopt a different approach, based on a variational Gaussian state wave function that is not a particle number eigenstate, but rather a superposition of states with different particle numbers. In this *Ansatz* pairwise correlations between the bosons are fully taken into account in the frame of the impurity. This translates to fully including the three-body correlations between two bosons and the impurity in the laboratory frame.

We emphasize that the functional form of the correlations in a Gaussian state is different from the correlation functions in the Jastrow-formalism [52], often used in condensed-matter physics, which was, for example, also employed to describe Bose polarons in Refs. [28,53]. In our case, the covariance matrix, which characterizes the correlations, is optimized variationally without restrictions on the functional form of the correlations.

In the following we will now highlight our various findings.

1. Gaussian states incorporate two- and three-body physics

First, we demonstrate that a Gaussian state combined with the Lee-Low-Pines transformation captures the Efimov effect exactly. To this end, we show that the EOMs of the two- and three-body problem can be retrieved exactly by linearizing the

EOMs for Gaussian states around the vacuum. The procedure of linearizing the EOMs is described in detail in Ref. [49] and here we retrace the main steps.

The EOMs for real-time evolution are given by [49]

$$i\partial_t \phi = \eta, \tag{19}$$

$$i\partial_t \Gamma = \Sigma^z \mathscr{H}\Gamma - \Gamma\mathscr{H}\Sigma^z. \tag{20}$$

Rewriting, without loss of generality, the correlation matrix Ξ as

$$\Xi = \begin{pmatrix} 0 & \delta\Xi \\ \delta\Xi^\dagger & 0 \end{pmatrix}, \tag{21}$$

the linearized EOMs of Γ can be rewritten in terms of $\delta\xi$,

$$i\partial_t \delta\Xi = \{D, \delta\Xi\} - i(S_0^\dagger \delta\mathscr{H} S_0)_{12}. \tag{22}$$

In this equation, D is obtained by symplectic diagonalization of $\mathscr{H}(\phi_0, \Gamma_0)$ by a matrix S_0 that satisfies $\Gamma_0 = S_0 S_0^\dagger$. The subscript 12 in Eq. (22) indicates the off-diagonal block in the Nambu basis.

Writing

$$\mathscr{H} = \begin{pmatrix} \mathcal{E} & \Delta \\ \Delta^\dagger & \mathcal{E}^* \end{pmatrix}, \tag{23}$$

we can diagonalize the EOMs around the vacuum, which yields

$$i\partial_t \delta\Xi = -i\Delta + \delta\Xi\mathcal{E}^* + \mathcal{E}\delta\Xi. \tag{24}$$

The variables η, $\mathcal{E}$, and Δ are functions of the quantities

$$G_{k_1 k_2 l} = \langle \delta\hat{\psi}^\dagger_{k_2 l m}, \delta\hat{\psi}_{k_1 l m}\rangle, \tag{25}$$

$$F_{k_1 k_2 l} = (-1)^m \langle \delta\hat{\psi}_{k_1 l -m} \delta\hat{\psi}_{k_2 l m}\rangle. \tag{26}$$

Their explicit form is given in Appendix C. Note that despite the fact that the right-hand sides of Eqs. (25) and (26) contain the angular momentum label m, the matrix elements of $\boldsymbol{G}$ and $\boldsymbol{F}$ are independent of m.

Finally, expanding to first order in $\delta\phi$ and $\delta\Xi$ gives

$$i\partial_t \delta\phi_k = \frac{k^2 \delta\phi_k}{2\mu_r} + \frac{gk}{2\pi^2}\int_{k'} k' \delta\phi_{k'}, \tag{27}$$

$$\begin{aligned} i\partial_t \delta\Xi_{k_1 k_2 l} =& \delta\Xi_{k_1 k_2 l}\frac{k_1^2 + k_2^2}{2\mu_r} + \frac{g}{2\pi^2}\delta_{l,0} k_2 \int_k k\, \delta\Xi_{k_1 k 0} \\ &+ \frac{g}{2\pi^2}\delta_{l,0} k_1 \int_k k\, \delta\Xi_{k k_2 0} + i\frac{k_1 k_2 (l+1)}{M(2l+1)}\delta F_{k_1 k_2 (l+1)} \\ &+ i\frac{k_1 k_2 l}{M(2l+1)}\delta F_{k_1 k_2 (l-1)}. \end{aligned} \tag{28}$$

Since $\delta F = i\delta\Xi$ after linearizing around the vacuum, it is evident that these equations exactly correspond to the EOMs for the two- and three-body problem: Eqs. (17) and (18). This shows that Gaussian states indeed fully capture the Efimov effect.

2. Cooperative binding with Gaussian states

We now turn to demonstrating the cooperative binding effect. Since a Gaussian state is not a particle number eigenstate, but a superposition of those, we cannot fix the particle number N, but instead we fix its expectation value $\langle\hat{N}\rangle$, given by

$$\langle \mathrm{GS}|\hat{N}|\mathrm{GS}\rangle = |\boldsymbol{\phi}|^2 + \mathrm{Tr}(G). \tag{29}$$

We aim to show that $E_{\mathrm{bind}}/\langle\hat{N}\rangle$ grows monotonically with $\langle\hat{N}\rangle$, which is a strong indication that also E_{bind}/N grows with N. To keep the average number of particles fixed during the imaginary-time evolution, we include a dynamically changing chemical potential. We find that during the optimization with fixed average particle number, the coherent part of the wave function approaches zero, leaving a purely Gaussian state. This is not surprising since this allows for the maximum amount of correlation between the particles.

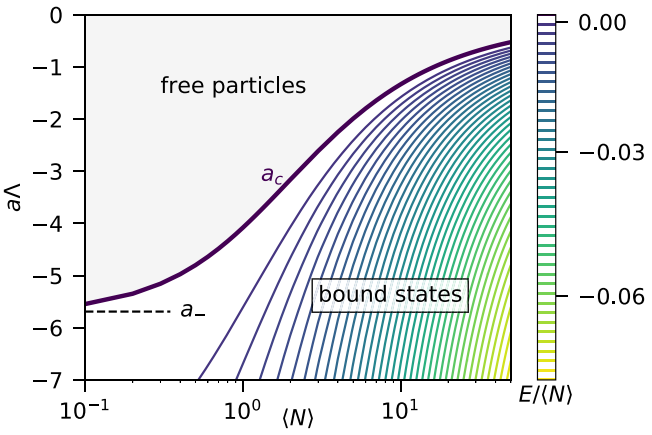

FIG. 2. Contour plot of the energy per particle $E/\langle N\rangle$ as a function of the number of particles $\langle N\rangle$ and the scattering length a in terms of the three-body parameter Λ for $M/m = 6/133$. The energy is given in units of Λ^2/M. The bold line indicates the critical scattering length at which a bound state first appears. The figure is also shown in our related work [45].

In Fig. 2 we show a contour plot of the energy per particle as a function of $\langle\hat{N}\rangle$ and a. The bold line indicates the scattering length a_c where the energy per particle becomes negative and bound-state formation sets in. Note that since the Hamiltonian conserves particle number, a_c is a smooth line only due to a classical average over different particle number sectors. As discussed above, in the limit of $\langle\hat{N}\rangle$ going to zero, we recover the three-body Efimov effect. We therefore observe that in this limit, $a_c \to a_-$.

As $\langle\hat{N}\rangle$ is increased, a_c monotonically decreases in magnitude. Importantly, at fixed scattering length the energy $E_{\mathrm{bind}}/\langle\hat{N}\rangle$ monotonically increases with $\langle\hat{N}\rangle$, as soon as $\langle\hat{N}\rangle$ is sufficient to lead to bound-state formation. This clearly demonstrates cooperative binding, i.e., the ability of the bosons to support each other's binding to the impurity. This result is in correspondence with recent work based on a stochastic variational approach by Blume [54] that also shows a strongly increasing energy as a function of particle number for an impurity immersed in a Bose gas.

As discussed above, it is important to emphasize that our method is variational not for fixed N but for fixed $\langle\hat{N}\rangle$. This means that the ground-state energy we find for a given average $N = \langle\hat{N}\rangle$ may be lower than the lowest particle number eigenstate of N particles. In fact, exactly because of the

property that E_{bind}/N increases with N, it is beneficial in the optimization of the energy to have a larger spread in the particle number. The Gaussian form of the wave function does however restrict the particle number statistics, meaning not arbitrary superpositions of particle number eigenstates are allowed. The standard deviation of the particle number for the Gaussian states scales with $\langle\hat{N}\rangle$. This means that the particle number fluctuations do not become relatively small for large $\langle\hat{N}\rangle$, as is often the case in statistical physics and, e.g., for coherent states. Thus, even for large $N = \langle\hat{N}\rangle$, the energy found with Gaussian states may be significantly lower than the particle number eigenstate of N particles. Altogether, even though there are subtleties to be aware of, none of them discount our evidence for the cooperative binding effect.

One obvious question is whether a_c goes to zero if $\langle\hat{N}\rangle$ goes to infinity, i.e., would an infinitely weak attraction already enable bound-state formation? A hint of the answer to this question is provided by the insight that the cooperative binding effect is fully driven by the $\hat{\mathcal{H}}_{\text{QLLP}}$ term originating from the kinetic energy of the impurity. A lower bound on $|a_c|$, which is quite general and in particular independent of the variational method, can therefore be derived by setting the kinetic energy of the impurity to zero. In this case the Hamiltonian becomes

$$\hat{\mathcal{H}} = \sum_{lm}\int_k \frac{k^2}{2m}\hat{b}^\dagger_{klm}\hat{b}_{klm} + \frac{g}{2\pi^2}\int_{k_1}\int_{k_2} k_1k_2\hat{b}^\dagger_{k_100}\hat{b}_{k_200}. \quad (30)$$

While this formally corresponds to a Hamiltonian of bosons interacting with a infinitely heavy impurity, there is an important subtlety. Namely, the relation between the scattering length and the coupling constant is determined by the reduced mass of the problem. By solving the two-body problem corresponding to Eq. (30), where the reduced mass is m, one finds an expression for the scattering length a_{eff} in this effective model,

$$g^{-1} = \frac{m}{2\pi a_{\text{eff}}} - \frac{m\Lambda}{\pi^2}. \quad (31)$$

In the spectrum of the Hamiltonian (30) a bound state appears precisely when $a_{\text{eff}} = -\infty$. Inserting this condition into Eq. (31) and comparing with Eq. (4) immediately yields a limiting scattering length in the original model

$$a_{c,\text{lim}} = -\frac{\pi M}{2m\Lambda}. \quad (32)$$

This is a bound of the lowest possible scattering length for which a bound state can appear. For Li-Cs this value is given by $a_{c,\text{lim}} = -0.07\Lambda^{-1}$. As can be seen in Fig. 2, this limit is only approached extremely slowly and might in fact not be reached by a Gaussian state *Ansatz*. In other words, the scattering length at which the most deeply bound Efimov state can form fulfills $a_-^{(\text{min})} \leqslant a_{c,\text{lim}}$. We again emphasize that this limit is fundamental and independent of the variational method. With more advanced *Ansätze* the limit can only be approached faster or more closely. In contrast, the limit will depend on the form of the interaction potential. The fact that we find $|a_c| < \Lambda^{-1}$ with Λ^{-1} on the order of the van der Waals length indicates that nonuniversal physics will become relevant in the description of a_c.

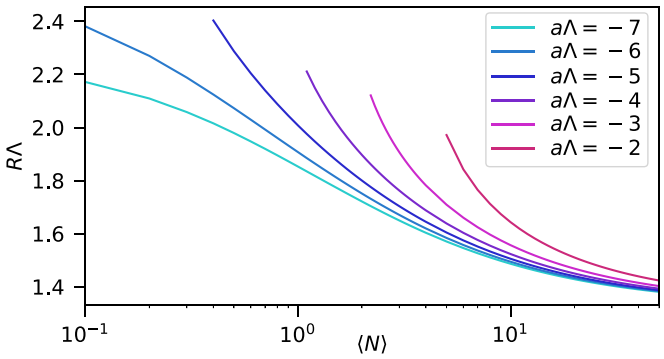

FIG. 3. Spatial extent R, defined by Eq. (33), of an Efimov cluster as a function of the number of particles $\langle\hat{N}\rangle$ for different scattering lengths $a\Lambda$ (indicated by color). The lines terminate when the bound states disappear into the continuum (see Fig. 2). The mass ratio is $M/m = 6/133$.

From a comparison with Table I, it is evident that $a_{c,\text{lim}}$ is approximately two orders of magnitude smaller than a_-. Note that such a minimal required scattering length to form an Efimov cluster does not exist for the homonuclear case, since there the pairwise interactions between all of the participating particles drive the cluster formation.

The increase in binding energy as a function of particle number and scattering length shown in Fig. 2 is accompanied by a decrease in the spatial extent of the Efimov clusters, which we define as

$$R = \sqrt{\frac{\langle\hat{N}\rangle}{\langle\int d\boldsymbol{k}\,\boldsymbol{k}^2\hat{b}^\dagger_{\boldsymbol{k}}\hat{b}_{\boldsymbol{k}}\rangle}}. \quad (33)$$

As shown in Fig. 3, the size of the Efimov clusters monotonically decreases as a function of a and $\langle\hat{N}\rangle$. It is evident that these cooperative Efimov clusters are tightly bound, with $R\Lambda$ being of order 1. Note that R parametrizes the average distance of the bosons to the impurity and not the distance of the particle farthest away. This means that the total extent of the Efimov cluster wave function can be much larger than described by R, especially close to a_c.

Finally, we corroborate our qualitative explanation of the mechanism underlying cooperative binding with quantitative numerical results. We have explained before that the impurity-mediated interaction between the bosons, described by the $\hat{\mathcal{H}}_{\text{QLLP}}$ in the Hamiltonian, follows from a reduction of the kinetic energy of the impurity. In Fig. 4 we plot the relative values of the energetic contributions to the problem, i.e., the kinetic energy of the bosons $E^{(\text{bos})}_{\text{kin}}$, the kinetic energy of the impurity $E^{(\text{imp})}_{\text{kin}}$, and the interaction energy E_{int}, as a function of the scattering length for various particle numbers $\langle N\rangle$. Whereas the ratio between the bosonic kinetic energy and the interaction energy only changes marginally when the number of particles is increased, the kinetic energy of the impurity relative to the interaction energy can decrease by more than a factor 2. Thus, it becomes apparent that the reduction of the kinetic energy of the impurity compared to the interaction energy is indeed the driving force of the cooperative binding mechanism. Note that the kinetic energy of the impurity decreases in relative but not in absolute terms when more bosons

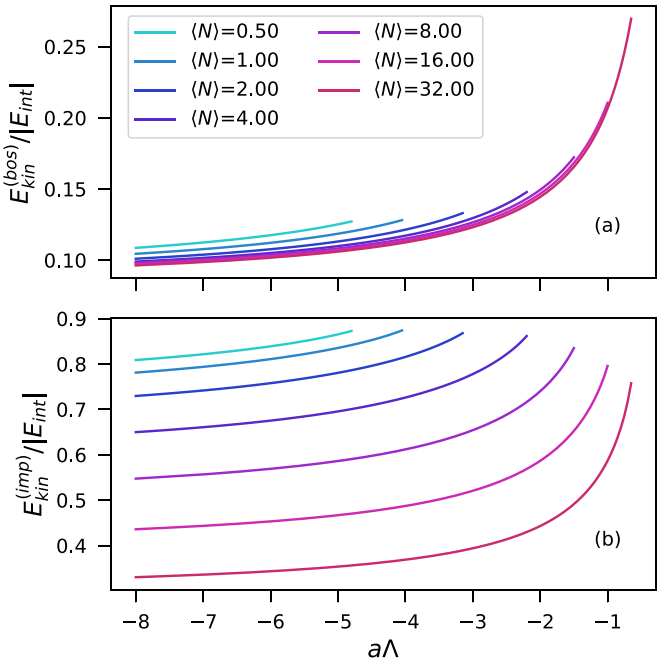

FIG. 4. Kinetic energy of (a) the bosons and (b) the impurity compared to the total interaction energy, as a function of the scattering length a (in terms of Λ), for several values of $\langle N\rangle$ and $M/m = 6/133$. The lines terminate when the bound states disappear into the continuum (see Fig. 2). The legend in (a) corresponds also to (b).

are added. Indeed, adding more bosons leads to tighter binding and therefore larger kinetic zero-point energy. Furthermore, the ratio between the kinetic and the interaction energy is not universal; it will depend on the shape of the potential. However, we believe that the general trend of the decreasing relative impurity kinetic energy for increasing particle number is a universal phenomenon.

The cooperative mechanism can also be interpreted in terms of an increase of the reduced mass of the system. For example, if a boson scatters on an impurity-boson bound state, this system has a larger reduced mass than the system of a boson scattering with a free impurity. However, the interaction potential remains the same, meaning that forming a bound state in the former system is easier than in the latter. This is clearly related to our explanation in terms of the impurity kinetic energy. Whereas in the case of a dimer state the impurity needs to completely compensate for the momentum of the boson it is bound to, in a trimer the bosons partially compensate for each other's momentum. This means that the impurity kinetic energy per boson is decreased.

3. Further aspects

The Efimov clusters are inherently unstable due to recombination into deeply bound molecular states that are not included in our model. Because of this rapid recombination, the specific structure of these clusters is not relevant for experiments, which is why we refrained from discussing it in detail. Instead, the main interest of this work is to show that the polaron, as discussed in the next section, can decay into Efimov clusters, a process independent of their microscopic structure. For this polaronic instability the cooperative binding effect is essential and this has hence been our main focus here.

The bound states that are formed for $N \gg 1$ are very tightly bound (as shown in Fig. 3) and the results we obtain in Figs. 2–4 are therefore not universal. Indeed, universality breaks down due to the piling up of bosons around the impurity. The cooperative binding mechanism ultimately leading to this breakdown is universal though, since the driving $\hat{\mathcal{H}}_{\mathrm{QLLP}}$ term is independent of the interaction potential.

The accumulation of bosons on the impurity can be prevented or limited by interboson repulsion. Due to the tightly bound nature of the bound states, not only the interboson scattering length but also the range of the interboson interactions will play an important role. As a result, a simple contact interaction will not be sufficient to describe this effect and more realistic potentials will need to be employed. Whether ultimately van der Waals universality [55–61] persists even for deeply bound states and states with more particles [62] remains an interesting open question.

Furthermore, also using a two-channel model, where the interaction between the impurity and the bosons is modeled by a coupling to a closed molecular channel, may modify the results. Especially in the closed-channel-dominated limit only a single boson can interact with the impurity at a time, resulting in an effective three-body repulsion [17]. Similar to a direct interboson repulsion, this may limit the size of Efimov clusters.

Finally, we note that the coherent part of the Gaussian state may also contribute to cooperative binding, although more weakly than the Gaussian part. This is due to the mixing between the coherent and the Gaussian term in the expectation value of $\hat{\mathcal{H}}_{\mathrm{QLLP}}$. In the next section this will become important, because only the coherent state term couples to the linear Fröhlich term in the Hamiltonian, crucial for polaron formation.

IV. EFIMOV EFFECT AND BOSE POLARON

We have shown that large and strongly bound Efimov clusters already form at small negative scattering lengths. The ground state in our system is therefore not the Bose polaron, but a state where all particles are bound to the impurity. This immediately raises questions concerning the fate of the polaron. Does a polaron state still exist and if yes, will it still be stable? Can it decay into the cooperative Efimov clusters? Finding answers to these questions is the aim of this section.

A. Stable and metastable polarons

We are now in the position to discuss the spectrum shown in Fig. 1 in more detail. Starting at the left of this figure, as discussed below Eq. (32) in the preceding section, there is a minimum scattering length $a_-^{(\min)} \leqslant a_{c,\mathrm{lim}} < 0$ required to form any Efimov cluster. As a result, for $a > a_-^{(\min)}$ the polaron remains the ground state of the Hamiltonian. However, $a_-^{(\min)}$ can be very small for light impurities, yielding only a small region where the polaron is truly stable.

The first clusters that form at $a_-^{(\min)}$ contain an exceedingly large number of particles. Since smaller clusters are not stable yet, all particles required for the bound-state formation need

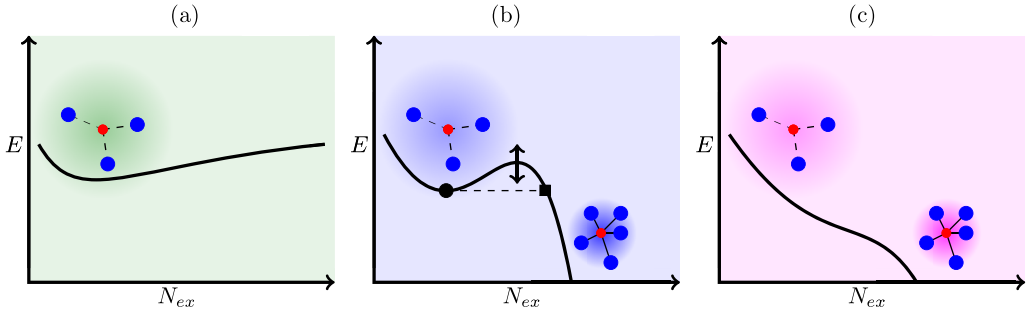

FIG. 5. Illustration of the energy landscape of the extended Fröhlich model (1) as a function of the number of excitations N_{ex} surrounding the impurity at a fixed density and scattering length in the (a) stable polaron, (b) metastable polaron, and (c) unstable polaron regimes, which correspond to the regimes shown in Fig. 1. In the stable polaron regime, there are no Efimov clusters to decay into, in the metastable regime there is a barrier protecting the polaron from this decay, and in the unstable regime this barrier has completely disappeared. The black circle and square in (b), connected by the dashed line, are of relevance for Fig. 7.

to come together without the possibility to cascade through long-lived intermediate states. Since cold atomic gases are dilute, the rate of the required N-body scattering processes is extremely small. Therefore, the polaron state, which at small scattering lengths is accompanied only by a relatively small and long-range deformation of the condensate, will not experience rapid decay into these clusters and remain relatively long-lived beyond $a_-^{(\mathrm{min})}$.

It can also be understood in a formal way from the Hamiltonian why the polaron should remain a stable state for weak interactions. For small scattering lengths and a small number of excitations in the polaron cloud, the contribution of the $\hat{\mathcal{H}}_{\mathrm{QLLP}}$ term in the Hamiltonian is negligible. Moreover, at negative scattering lengths no two-body bound states can be formed yet. This implies that the quadratic kinetic energy term in Eq. (3) dominates over the quadratic interaction terms. The remaining model thus closely resembles the original Fröhlich model where a linear term drives polaron formation and a quadratic kinetic energy term counteracts this process. This model has a minimum of the energy as a function of particle number, as graphically illustrated in Fig. 5, where the energy landscape of the Hamiltonian is plotted as a function of the number of excitations around the impurity for fixed background density.

For $0 > a > a_-^{(\mathrm{min})}$ [Fig. 5(a)], the polaron is the global minimum of the energy landscape and hence stable. When $a_-^{(\mathrm{min})}$ is crossed the local minimum is not immediately affected, since the barrier protecting it is still large and a bound state can be formed only for a very large number of excitations. The correspondence to the original Fröhlich model persists as long as the particle number corresponding to the local minimum is sufficiently small for the quartic term to remain of minor importance. This changes, however, for large scattering lengths or densities. In this case the particle number at the polaron minimum found from the simplified model is so large that the quartic term can no longer be neglected. When this occurs [as depicted in Fig. 5(b)], the barrier protecting the polaron from decaying into Efimov clusters starts to disappear. Eventually, at the critical scattering length a^* the barrier completely disappears, resulting in the breakdown of the polaron, and one enters the regime illustrated in Fig. 5(c).

B. Breakdown of the polaron

Now we will discuss in more detail the process leading to the breakdown of the polaron. At the critical scattering length a^* where the instability occurs, the polaron state is a saddle point on the variational manifold. Therefore, the polaron state is no longer stable against a specific type of perturbations. These perturbations can be identified by computing the tangent vectors [36,63] on the variational manifold. The resulting processes represent single and double excitations on top of the Gaussian state. Thus, the polaron becomes unstable when a single or double excitation (or a linear combination thereof) can result in the formation of a bound state. Once a bound state is formed, the cooperative binding effect drives a cascade into more deeply bound states of ever increasing particle number. In a medium this is possible, since there is a coupling between the different particle number sectors: The polaron can draw particles from the medium. Eventually, this leads to the collapse of the system onto the impurity.

The value of the scattering length a^* can be calculated numerically as a function of the density. To this end, we use the following procedure. We start at small scattering lengths where the local minimum corresponding to the polaron can easily be identified. We then incrementally increase the coupling strength. In every step the polaron energy and wave function are calculated with iterated Bogoliubov theory, using the polaron wave function at the previous scattering length as a starting point. As the critical scattering length a^* is reached, the barrier preventing the polaron from decaying into many-body bound states disappears, leading to the breakdown of the impurity.

1. Polaronic instability and shift of the Efimov resonance

In Fig. 6 we show a^* as a black solid line as a function of the interparticle distance $n_0^{-1/3}\Lambda$ for two values of the interboson scattering length $a_B\Lambda = 0.01$ and 0.1. Additionally, we show the spectral weight Z of the polaron as a colormap. It is given by the overlap of the wave function with the unperturbed state, which for a Gaussian state can be written as

$$Z = \frac{\exp[-\Phi^\dagger(\Gamma + I)^{-1}\Phi]}{\sqrt{\det\left(\frac{\Gamma+I}{2}\right)}}, \tag{34}$$

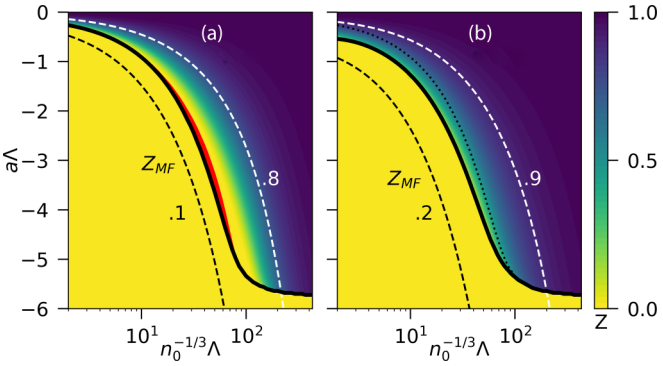

FIG. 6. Polaron quasiparticle weight Z as a function of the interparticle distance $n_0^{-1/3}\Lambda$ and scattering length a for mass ratio $M/m = 6/133$. Two different interboson scattering lengths are chosen: (a) $a_B\Lambda = 0.01$ and (b) $a_B\Lambda = 0.1$. The black solid line indicates the critical scattering length a^* at which the polaron breaks down. The dotted line in (b) is a guide to highlight the difference between (a) and (b) and corresponds to the solid line in (a). The red region close to the solid line in (a) is a region of dynamic instability. The dashed lines indicate contours of the quasiparticle weight Z_{MF} obtained from mean-field theory.

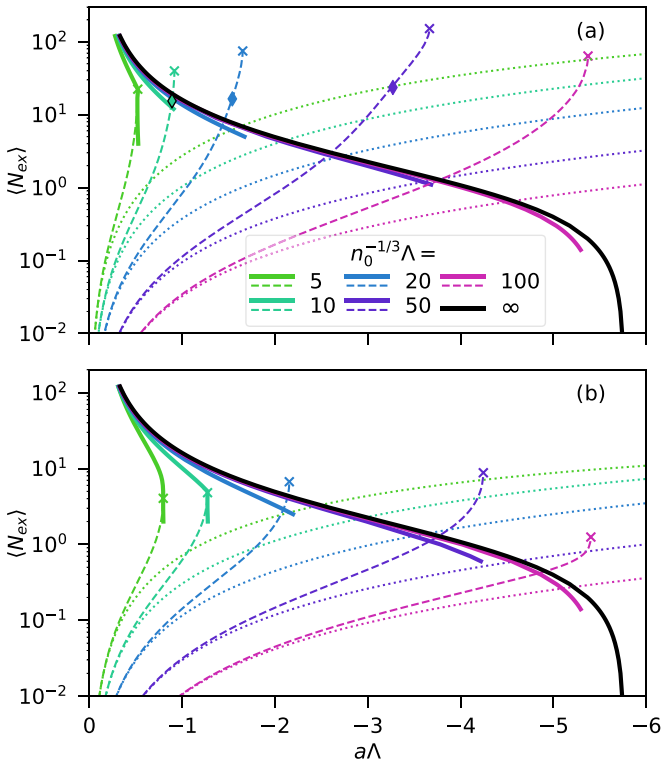

FIG. 7. Quantitative analysis of the polaronic instability mechanism. The number of excitations $\langle \hat{N}_{\mathrm{ex}}\rangle$ contained in the polaron cloud (Gaussian state, dashed lines; coherent state, dotted lines) compared to the critical number of particles needed for bound-state formation (solid lines) in the presence of a background BEC is plotted versus the scattering length $a\Lambda$. The interboson scattering length is given by (a) $a_B\Lambda = 0.01$ and (b) $a_B\Lambda = 0.1$. The black solid line indicates the critical particle number for bound-state formation in the absence of a background BEC, corresponding to the line of a_c displayed in Fig. 2. Crosses indicate where the polaron is destabilized in the Gaussian state *Ansatz*. Diamonds indicate the position beyond which a dynamical instability occurs. The legend in (a) also applies to (b).

where I is the identity matrix. Experimentally, Z can be measured using injection rf spectroscopy [18,19].

First we consider the low-density limit. Here we find that $a^* \to a_-$, i.e., the polaron ceases to exist exactly at the three-body Efimov scattering length. This finding can be understood as follows. For small densities, the polaron cloud is extremely dilute, meaning the impurity is practically free. A bound state for a free impurity plus two excitations from the background can be formed when the first three-body bound state crosses the continuum, which precisely happens at a_-. This transition from a free impurity to a three-body Efimov state is accompanied by a sharp drop of the quasiparticle weight from 1 to 0.

As the density is increased, the polaron cloud surrounding the impurity is established containing excitations from the BEC. The formation of this polaron cloud has multiple consequences. First, as can be seen from Fig. 6, it leads to a reduction of the quasiparticle weight for increasing density. Second, due to the increased density around the impurity, scattering of two particles on the polaron can lead to the formation of clusters of more than three particles. Importantly, due to the cooperative binding effect, these larger clusters can already be formed at scattering lengths smaller than a_-. Therefore, $|a^*|$ shifts to smaller scattering lengths as the density increases. This argument suggests the interpretation of the polaronic instability as a many-body shifted Efimov resonance [45], where the polaron takes over the role of the free impurity as a collision partner of two *additional* bosons. This reasoning also implies that the timescale associated with this instability is on the same order as the timescale associated with three-body recombination.

One fascinating aspect of this finding is that the shift of a^* is continuous. While the average over particle number sectors in our discussion of cooperative binding in Sec. III and Fig. 2 was purely classical, here the Hamiltonian coherently couples different particle number sectors. This means that instead of obtaining a classical average over three-, four-, and five-body Efimov states, clusters formed in the presence of a background BEC contain a quantum mechanical superposition of different particle states. This originates from the quantum coherent nature of the BEC giving rise to the linear Fröhlich term in the Hamiltonian and highlights an intriguing aspect of chemistry in a medium of a quantum nature.

2. *Mechanism of the polaronic instability*

We now study quantitatively the mechanism underlying the polaronic instability. To this end, it is useful to introduce the relevant length scales of the problem: the size of the Efimov trimer, which is on the order of a_-; the average interparticle distance, parametrized by $n_0^{-1/3}$; and the size of the polaron cloud, which is determined by the modified healing length of the BEC $\xi_B = (8\pi n_0 a_B \mu_r/m)^{-1/2}$ [30].

In Fig. 7 we show the number of excitations in the polaron cloud computed with a Gaussian (coherent) state *Ansatz* as a function of the scattering length as dashed (dotted) lines. As solid lines (color indicating various background densities) we show the critical particle number needed to form a bound

state with an energy lower than the polaron energy at the given scattering length and background density. In terms of the illustration in Fig. 5(b), we compare the number of particles contained in the polaronic excitation cloud (black circle) with the number of particles that is needed to form a bound state of at least the polaron energy (black square).

The crosses at the end of the dashed lines indicate the scattering length a^* of the polaron instability. This instability is not captured by the coherent state *Ansatz*. In between the crosses and the diamonds appearing on some lines we find regions of dynamical instability, discussed in more detail below. The black line in this figure shows the critical scattering length for bound-state formation as a function of particle number in the absence of a background BEC, such as shown in Fig. 2.

First we compare the results from the coherent and Gaussian state *Ansätze* (dotted and dashed lines). While they coincide for small a and $\langle \hat{N}_{\mathrm{ex}} \rangle$, for larger a the particle number of the polaron calculated using Gaussian states grows much more rapidly. This leads to a difference of one to two orders of magnitude close to the critical scattering length. Next we consider the solid lines, corresponding to the onset of bound-state formation. Based on the simplified illustration in Fig. 5(b), one would expect that the polaron instability would occur precisely when the dashed lines cross the solid lines. However, this is not the case. In the low-density regime, the dashed lines in fact continue after crossing the solid lines, meaning that the polaron remains stable even when containing more than enough particles to form a bound state. The crucial insight to understand this behavior is that in this regime $\xi_B \gg a_-$. Thus, even though the particle number in the polaron cloud is very large, the cloud is so extended that the number of particles within a volume set by a_- is still too small to facilitate bound-state formation. In contrast, in the high-density regime we find that the instability exactly occurs when the dashed lines hit the solid lines. In this regime the healing length ξ_B that determines the size of the polaron cloud is comparable to or smaller than the extent of the Efimov state. Therefore, a bound state can be formed immediately when the polaron cloud contains the required number of particles. In the intermediate-density regime, there is a crossover between these two regimes. Consistent with this interpretation, we find that the larger the a_B, and thus the smaller the ξ_B, the lower the density at which the transition occurs.

We see that the scattering length of the instability $|a^*|$ (indicated with the crosses in Fig. 7) shifts towards smaller values for larger densities. From Fig. 7 it appears that the main mechanism of this shift is an increase of the number of excitations in the polaron cloud as a function of background density (horizontal shift of dashed lines). Another contribution comes from the vertical shift of the solid lines. This shift is due to the linear Fröhlich term in the Hamiltonian, which leads to the stabilization of the coherent polaron cloud due to the background density. This coherent part of the wave function also participates in the cooperative binding, leading to a downward shift of the solid lines. This effect is in turn slightly counteracted by interbosonic repulsion and the associated modification of the Bogoliubov quasiparticle dispersion [compare Figs. 7(a) and 7(b)], which plays the strongest role for large densities and a_B.

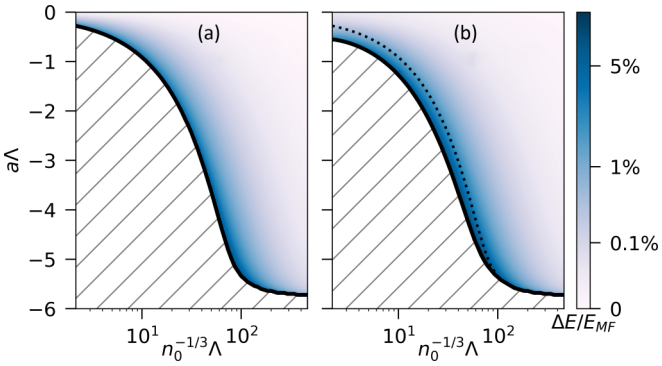

FIG. 8. Relative energy difference $(E - E_{\mathrm{MF}})/E_{\mathrm{MF}}$ between the energy E obtained from the Gaussian state and mean-field theory E_{MF} as a function of the density n_0 and scattering length a for mass ratio $M/m = 6/133$. Two different interboson scattering lengths are chosen: (a) $a_B\Lambda = 0.01$ and (b) $a_B\Lambda = 0.1$. The black solid lines indicate a^*. The dotted line in (b) corresponds to the solid line of (a) and is shown to more clearly indicate the difference between (a) and (b). Note that the color scale is not linear but cubic.

We note that in our framework the most important role of a_B is to determine the healing length. If we compare Figs. 7(a) and 7(b) we see that the healing length mainly determines the number of particles in the polaron cloud. This is also reflected in the quasiparticle weight Z in Figs. 6(a) and 6(b).

C. Further aspects

1. *Properties of the metastable polaron*

Above we have focused on the instability of the polaron described by Gaussian states. Another interesting question is how much the properties of the polaron are altered compared to the coherent state approach [16] in the regime where the polaron is metastable. In Fig. 8 we plot the energy difference $\Delta E = E - E_{\mathrm{MF}}$ between the polaron energy calculated from Gaussian states E and coherent states E_{MF}, which is given by

$$E_{\mathrm{MF}} = \frac{2\pi n_0}{\mu_r\left(a^{-1} - a_0^{-1}\right)}. \tag{35}$$

The resonance shift parameter a_0 [16] is defined in Appendix A.

Remarkably, the effect on the energy appears to be very small. A significant correction to the polaron energy only appears close to the instability, although still limited to less than 10%. Hence, while introducing correlations in the variational *Ansatz* leads to a decrease in spectral weight and destabilization at some point, the energy of the polaron is still very well described using mean-field theory. This reflects the general notion that while variational energies may work well, the same may not apply for the wave functions.

We have already seen by comparing the dashed and dotted lines in Fig. 7 that the numbers of excitations in the polaron cloud obtained from coherent or Gaussian states are very different. While they still coincide for small particle numbers and scattering lengths, where the quartic $\hat{\mathcal{H}}_{\mathrm{QLLP}}$ term has only a small contribution, this term starts to be important for scattering lengths approaching a^*. As a result, the difference between Gaussian and coherent states rapidly increases. This

finding is also directly associated with the much smaller Z factor for the Gaussian state result (see Fig. 6).

2. Dynamical instability

Our numerical results show a region of dynamical instability [red area in Fig. 6(a)]. A dynamical instability occurs when the variational parameters correspond to a minimum on the variational manifold, but to a saddle point with respect to its tangent space. To identify the presence of the dynamical instability, we linearize the real-time EOMs around the minimum found from iterated Bogoliubov theory. The system is stable when the symplectic diagonalization of the linearized time-evolution operator yields only positive real eigenvalues. However, in the case of a dynamical instability, one finds imaginary eigenvalues corresponding to a negative direction in the Hessian. In the real-time evolution the imaginary eigenvalues manifest as an instability with exponentially growing populations of the excitation modes.

Importantly, the dynamical instability indicates that the variational manifold is no longer suitable to describe the state of the system. Hence, to fully describe the dynamics in this regime, even higher-order correlations would need to be incorporated in the model.

In Fig. 6 the dynamical instability occurs in the small red region attached to the solid line at intermediate densities for $a_B\Lambda = 0.01$. This is exactly the region where the polarons are very large in number of particles and extent, but where the density at the impurity is too small to lead to bound-state formation. A dynamic instability was also found for the Bose polaron within the coherent state description in Ref. [64]. Although the character and position of this instability is different from the one we find here, the origin may be related.

A dynamical instability can also be found when extending our plots to higher density. Here our results are however no longer valid, because when $n_0^{-1/3}\Lambda > 1$, one can no longer speak of universal long-range physics, and short-range physics will dominate the behavior of the system. This corresponds to interparticle distances comparable in scale to the length scale of the interaction potentials. In gases of cold atoms the typical densities are orders of magnitude away from this limit.

3. Dependence on the mass of the impurity

Finally, we study the mass dependence of our results. To this end we investigate a significantly different mass ratio by choosing a ^{6}Li-^{23}Na system as an example. In this case we fix the interboson scattering length to $a_B\Lambda = 0.1$. We show a^*, the polaron energy, and the quasiparticle weight as a function of the interparticle spacing $\sim n_0^{-1/3}$ in Fig. 9.

The most obvious difference compared to the ^{6}Li-^{133}Cs case is the change in the scale of the relevant scattering lengths. Already from the few-body problem we know that $|a_-|$ increases strongly when the mass ratio m/M decreases (see Table I). As evident from Fig. 9, we find that the same holds in the many-body case. This behavior is also reflected in a change in the scale of the relevant densities. This is not surprising, however, considering that it is the dimensionless ratio between the interparticle distance and the size of the Efimov state (scaling with a_-), which is relevant for the

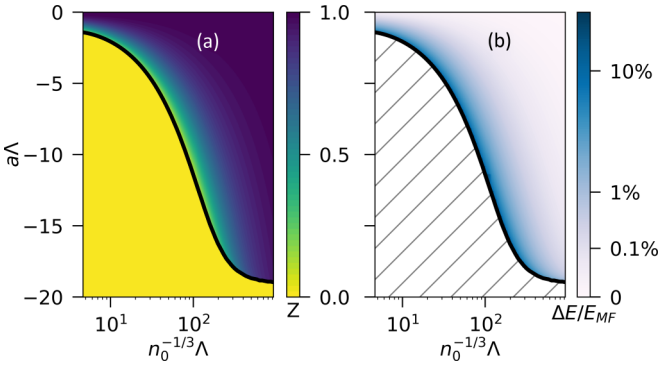

FIG. 9. (a) Quasiparticle weight Z and (b) fractional energy difference $(E - E_{\mathrm{MF}})/E_{\mathrm{MF}}$ as a function of the density n_0 and scattering length a for mass ratio $M/m = 6/23$ and $a_B\Lambda = 0.1$. Solid lines indicate the critical scattering length a^*.

physics. Except for these changes in scale there are no striking physical differences between the Li-Na and Li-Cs systems. One small quantitative difference is the difference between the polaron energy predicted by the Gaussian state and mean-field approaches. This difference is slightly larger for the Li-Na mass ratio than for Li-Cs.

V. DISCUSSION AND EXPERIMENTAL PROPOSAL

A. Limitations of our approach

Now we consider the limitations of our approach. First, we have limited ourselves to scattering lengths a_B sufficiently small to preserve the validity of the Bogoliubov approximation. To ensure this, we tested that going beyond the Bogoliubov approximation with these interboson scattering lengths only leads to small deviations from our results (less than 10% for a^*). Going beyond the Bogoliubov approximation comes with the challenge of greatly increasing numerical complexity and the necessity and difficulty to properly regularize the interboson interactions. Detailed studies dealing with these issues are left for future work. We expect that for light impurities experimental regimes can be found where our results qualitatively hold, despite the fact that for realistic experiments $a_B\Lambda$ will be of order one. In the case of large a_B, however, we expect that the cooperative binding will be strongly suppressed due to the interboson repulsion. Furthermore, for heavier impurities the cooperative binding effect is much weaker, meaning that the value of $a_B\Lambda$ needed to suppress the effect is also much smaller than for light impurities. This makes it unlikely that the polaronic instability can be observed experimentally for heavy impurities. In these scenarios, we expect a smooth crossover from the attractive polaron into dimers or small Efimov clusters [15,17].

Second, we have studied the properties of local energy minima on our variational manifold only using imaginary-time evolution. For that reason we could in particular not go beyond a^* to study, e.g., higher-order Efimov states or the repulsive polaron. Furthermore, calculating spectral functions with a Gaussian state variational manifold is challenging for various reasons. Therefore, the fate of the polaron branch in our model beyond the instability remains an important open direction of study. We consider it unlikely that the polaron branch will completely disappear and we hypothesize that it

will be broadened due to the decay into the Efimov clusters. We expect that the resulting width of the spectral line will be inversely proportional to the timescale of the decay, likely determined by, and similar to, the timescale of three-body recombination.

Third, our approach considers up to three-body correlations between two bosons and the impurity. It is thus a natural question to ask how our results would generalize when including even higher-order correlations. We expect that when up to N-body correlations are included, the value of a^* would asymptotically connect to the resonance of the N-body Efimov cluster. Due to the cooperative binding effect, its absolute value would in turn be smaller than $|a^*|$ obtained in this work. As discussed before, however, we do not expect the polaron branch in the spectrum to suddenly disappear at the point of instability, but rather expect it to be broadened by the timescale associated with its decay. Since cold atomic gases are typically very dilute, rates for N-body scattering in experiments are typically highly suppressed for $N > 3$ [43]. As a result, we expect that the inclusion of beyond-three-body correlations should not have a strong effect on most observables.

Finally, we note that our results may not fully apply to closed-channel dominated Feshbach resonances, because we use a single-channel model. Effective repulsive three-body interactions present in such systems [17,35] could counteract the cooperative binding, but are not included in our model.

B. Comparison to other theoretical approaches

We have already quantitatively compared some of our results with the mean-field approach using coherent states [16,30,53,64]. On the conceptual side, the most drastic difference is that the coherent state approach does not include three-body correlations. Since these are crucial to describe the Efimov effect, the coherent state approach completely misses the cooperative binding effect and the presence of the Efimov clusters. In the coherent state model, the polaron is the ground state for all negative scattering lengths and even beyond unitarity [16]. The polaron energy then diverges at the positive scattering length a_0 as a result of a large number of excitations piling up on the impurity. The scattering length a_0 can be interpreted as defining a shifted version of the unitarity point, i.e., the point where a two-body bound state enters the continuum.

In contrast to the Gaussian state approach, where a^* is shifted to *smaller* coupling strengths compared to a_-, the defined a_0 implies a shift to stronger coupling strengths. This highlights also the different mechanisms governing these shifts. For Gaussian states the shift is predominantly caused by the cooperative binding effect, whereas the interboson repulsion on the Bogoliubov level is responsible for the shift in the case of coherent states.

Interboson interactions play an important role in our model as they set the healing length of the BEC, and hence the extent of the polaron cloud. Guenther *et al.* [30] showed that explicitly including interboson interactions can prevent the collapse of an infinite number of bosons onto the impurity (see also Ref. [31]). However, this effect only plays a role for sufficiently high densities in the polaron cloud. In principle, the full inclusion of explicit interboson repulsion will also limit the number of particles that an Efimov cluster can host. However, for the light impurities and small interboson scattering lengths considered in this work, the size of Efimov clusters for which this effect would play an important role is much larger than the size of the Efimov clusters into which the polaron will initially decay. Therefore, we expect that explicit interboson repulsion will not qualitatively change the critical scattering length at which the polaron instability occurs.

Using a renormalization-group approach [29], it was predicted that the polaron becomes unstable for a finite negative scattering length. This was attributed to phase and particle number fluctuations and no connection to the Efimov effect was made. Since the general picture of a polaronic instability at negative scattering lengths agrees with our results, it remains an interesting open question how the two pictures might be related.

In Refs. [15,17,41] the interplay between Efimov physics and Bose polaron formation was studied for a limited number of excitations from the BEC. For a mass ratio $m/M = 1$ a smooth crossover between the Bose polaron and the lowest-energy Efimov cluster was found [15,17], consistent with quantum Monte Carlo results [28]. In these studies the most deeply bound Efimov state contained a limited number of particles. In contrast, in our case the lowest-energy Efimov cluster contains an infinite particle number, and there can hence be no smooth crossover from the polaron into this state. This qualitative difference can be explained by the different mass ratios used and the effective three-body repulsion that is implicitly part of the two-channel model used in Refs. [15,17]. In Ref. [41] radio-frequency injection spectra were predicted for the same mass ratio we considered. However, since the number of possible excitations from the BEC in the employed diagrammatic approach was limited, the possibility of forming many-particle Efimov clusters was not included.

C. Experimental implementation

Our predictions have not yet been tested experimentally [18–20]. In experiments performed so far the impurities were at least as heavy as the bosons of the BEC, leading to a strong suppression of the Efimov effect. As a result, any Efimov features would only have been observable at very large negative or positive scattering lengths. In this work we focus on the example of ^{6}Li impurities in a BEC of ^{133}Cs, but for Li in Rb or K BECs, as also available in experiments [65,66], the results should be very similar.

The typical densities of BECs vary in the range of 10^{13}–10^{15} cm^{-3} [67]. Assuming the three-body parameter $\Lambda \approx l_{\mathrm{vdW}}^{-1}$ and a van der Waals length of Li-Cs of $45a_0$, this gives a regime of $n_0^{-1/3}\Lambda \sim 40$–$200$. This implies that the low- and intermediate-density regime of our results can readily be probed, and a clear shift of the Efimov resonance should be observable. In practice, tuning the density in the experiment for a given BEC may be difficult. However, the resonance position in a BEC could be compared with the resonance position in a thermal gas. The latter could then serve as a reference that should give results comparable to our low-density predictions.

For the specific case of the Efimov resonances observed for Li-Cs at positive Cs-Cs scattering length [59,68], an in-

teresting subtlety comes into play. In this case the resonance corresponding to the lowest-energy Efimov state is suppressed due to coupling to a shallow Cs_2 bound state. Therefore, the first observed Efimov resonance actually corresponds to the second Efimov state and it appears at a scattering length of around $-2000a_0$. If we use this Efimov resonance as the lowest resonance in our model, we find a larger three-body parameter $\Lambda^{-1} = 8\ l_{\mathrm{vdW}}$. By virtue of the larger size of the Efimov state, this implies that in fact the high-density regime of our results could be probed: $n_0^{-1/3}\Lambda \sim 5$–25. Moreover, for smaller mass ratios m/M such as ^{6}Li in a BEC of ^{23}Na, the value of a_- is naturally larger. As a result, $n_0^{-1/3}a_-$ is larger and higher dimensionless densities can be reached as well.

We propose combining two experimental approaches to test our predictions. The first approach would be to perform loss measurements such as regularly used to observe Efimov resonances [4,39,40,43,44,59,68]. In this case the magnetic field should adiabatically be ramped from weak to stronger interactions to form a polaron. Then, at a given final scattering length a, the magnetic field should be kept fixed and the loss arising from recombination should be measured. As this final scattering length is varied, one should observe an enhancement of the loss when a^* is reached. Whether this appears as a resonant feature or as the onset of a regime where three-body recombination is enhanced is an open question and subject of further study. Loss measurements may be more efficiently performed by using the recently introduced photoassociative ionization technique [69].

The second approach would be to perform rf injection spectroscopy such as used in Refs. [18,19] for lighter impurities. A clear drop in quasiparticle weight and a broadening of the polaron spectral line of the polaron should be observable as the scattering length of the polaron instability is approached and crossed. When doing ejection spectroscopy as in Ref. [20], the ground-state polaron is prepared in the initial state. In this case enhanced three-body loss due to Efimov cluster formation will be the most important observable. The formation of tightly bound Efimov clusters may also give rise to higher-frequency tails in the rf spectrum because of their large amount of kinetic energy.

In conclusion, observation of our theoretically predicted phenomena is in reach with current state-of-the-art experimental techniques.

VI. CONCLUSION AND OUTLOOK

In this work we used a variational Gaussian state *Ansatz* to describe the Bose polaron problem and the Efimov effect. We found that the cooperative binding caused by the Efimov effect leads to the formation of many-particle Efimov clusters. The cooperative binding is driven by the reduction of the kinetic energy of the impurity. Since the Efimov clusters are lower in energy than the Bose polaron, the polaron is not the ground state of the extended Fröhlich Hamiltonian but rather exists as a metastable excited state. This excited state loses its stability at a critical scattering length a^* that can be interpreted as a many-body shifted Efimov resonance.

We predicted that while the mean-field energy of the polaron is reliable up to the point where the polaron becomes unstable, the inclusion of interboson correlations leads to a strong decrease in the spectral weight. Our results can be experimentally probed by a combination of rf spectroscopy and three-body loss measurements of light impurities immersed in BECs. The parameter regimes discussed in our work are experimentally feasible, requiring systems that feature both a small interboson scattering length and a large boson-impurity scattering length. We expect our results to also hold, up to quantitative shifts, for slightly larger interboson scattering lengths.

Future interesting directions include the study of the real-time dynamics of the polaron [53,64,70] using Gaussian states. Certainly one aim should be to understand how Efimov cluster formation occurs in real time and whether indeed resonant behavior can be observed at the scattering length a^*. Furthermore, the scope of our results can be extended to multichannel models, finite polaron momentum [71,72], or explicit interboson repulsion. This will allow the study of closed-channel dominated resonances, the dispersion relation of the polaron, and the repulsive side of Feshbach resonances, respectively. Our methods can also be extended to rotating impurities [73–75] or bipolarons [76–78] to study the effect of induced interboson correlations in those systems.

It would be fascinating to explore further the connection to quenched BECs [6–14]. In the present work we have shown that the formation of a polaron cloud around an impurity can lead to a modification of Efimov physics. One natural question to ask is whether a similar effect occurs in BECs quenched to negative scattering lengths. While one can certainly not employ the language of polarons or polaron clouds in this case, it is still two-body and higher-order correlations between the bosons that make them cluster together more closely, which is also the essence of polaron physics. Hence, it will be interesting to explore whether a shift of Efimov resonances can also be observed in said scenarios. One way to explore such effects could be the application of the cumulant expansion method as described in Ref. [13,14] to negative scattering lengths.

Finally, it remains an interesting open question how similar the polaron instability is to the collapse of a BEC. In our model with bosonic interactions included on the Bogoliubov level, the single impurity induces a first-order phase transition of the entire system at $a_-^{(\mathrm{min})}$. Even though this is prevented in practice by explicit interboson repulsion, it still indicates that the impurity can have a profound effect on the medium. Furthermore, the study of how large an Efimov cluster in a medium can become before it leads to recombination and loss remains another open question. These questions highlight how the study of impurity physics can give new insights into the dynamics of quenched or collapsing BECs.

ACKNOWLEDGMENTS

The authors are thankful to T. Guaita, T. Shi, V. Colussi, and M. Parish for useful discussions. J.I.C. acknowledges funding from ERC Advanced Grant QENOCOBA under the EU Horizon 2020 program (Grant Agreement No. 742102). The authors acknowledge support from the Deutsche Forschungsgemeinschaft (German Research Foundation) under Germany's Excellence Strategy EXC-2111-390814868.

APPENDIX A: DEFINITIONS OF VARIABLES

In this Appendix we provide the definitions of the variables that are introduced in Eq. (3) by replacing the original bosons by Bogoliubov quasiparticles. The dispersion relation and operators are defined as

$$\omega_k = \sqrt{\frac{k^4}{4m^2} + \frac{g_B n_0 k^2}{m}}, \tag{A1}$$

$$\hat{a}_{\boldsymbol{k}} = u_k \hat{b}_{\boldsymbol{k}} - v_k \hat{b}^\dagger_{-\boldsymbol{k}}, \tag{A2}$$

$$u_k = \sqrt{\frac{1}{2}\left(\frac{\omega_k + g_B n_0}{\omega_k} + 1\right)}, \tag{A3}$$

$$v_k = \sqrt{\frac{1}{2}\left(\frac{\omega_k + g_B n_0}{\omega_k} - 1\right)}. \tag{A4}$$

The variables concerning the interaction of the impurity, W_k, $V^{(1)}_{k,k'}$, and $V^{(2)}_{k,k'}$, appearing in the Hamiltonian, as well as a_0 providing a mean-field shift of the scattering length due to the modified quasiparticle dispersion, are given by

$$W_k = \frac{k}{\sqrt{2m\omega_k}}, \tag{A5}$$

$$V^{(1)}_{k,k'} = \frac{W_k W_{k'}}{2} + \frac{1}{2(W_k W_{k'})}, \tag{A6}$$

$$V^{(2)}_{k,k'} = \frac{W_k W_{k'}}{2} - \frac{1}{2(W_k W_{k'})}, \tag{A7}$$

$$a_0^{-1} = \frac{2\Lambda}{\pi} - \frac{1}{\mu_r \pi}\int_0^\Lambda dk \frac{k^2 W_k^2}{\omega_k + \frac{k^2}{2M}}. \tag{A8}$$

APPENDIX B: THE QUARTIC LEE-LOW-PINES TERM

Here we give the explicit expression for the quartic $\hat{\mathcal{H}}_{\mathrm{QLLP}}$ term which originates from the Lee-Low-Pines transformation acting on the impurity momentum operator in the spherical wave basis. It reads

$$\begin{aligned}
\hat{\mathcal{H}}_{\mathrm{QLLP}} &= \iint d\boldsymbol{k_1} d\boldsymbol{k_2} \frac{\boldsymbol{k}_1 \cdot \boldsymbol{k}_2}{2M} \hat{b}^\dagger_{\boldsymbol{k_1}} \hat{b}^\dagger_{\boldsymbol{k_2}} \hat{b}_{\boldsymbol{k_1}} \hat{b}_{\boldsymbol{k_2}} \\
&= \frac{1}{2M} \sum_{l_1 l_2 m_1 m_2} \int_0^\Lambda \int_0^\Lambda dk_1 dk_2 \frac{k_1 k_2}{\sqrt{(2l_1+1)(2l_1+3)(2l_2+1)(2l_2+3)}} \\
&\quad \times [\sqrt{(l_1 - m_1 + 1)(l_1 + m_1 + 1)(l_2 - m_2 + 1)(l_2 + m_2 + 1)} \\
&\quad \times (2\hat{b}^\dagger_{k_1(l_1+1)m_1} \hat{b}^\dagger_{k_2 l_2 m_2} \hat{b}_{k_1 l_1 m_1} \hat{b}_{k_2(l_2+1)m_2} - \hat{b}^\dagger_{k_1(l_1+1)m_1} \hat{b}^\dagger_{k_2(l_2+1)m_2} \hat{b}_{k_1 l_1 m_1} \hat{b}_{k_2 l_2 m_2} - \hat{b}^\dagger_{k_1 l_1 m_1} \hat{b}^\dagger_{k_2 l_2 m_2} \hat{b}_{k_1(l_1+1)m_1} \hat{b}_{k_2(l_2+1)m_2}) \\
&\quad + \sqrt{(l_1 - m_1 + 1)(l_1 - m_1 + 2)(l_2 + m_2 + 1)(l_2 + m_2 + 2)} \\
&\quad \times (\hat{b}^\dagger_{k_1(l_1+1)(m_1-1)} \hat{b}^\dagger_{k_2(l_2+1)(m_2+1)} \hat{b}_{k_1 l_1 m_1} \hat{b}_{k_2 l_2 m_2} + \hat{b}^\dagger_{k_1 l_1 m_1} \hat{b}^\dagger_{k_2 l_2 m_2} \hat{b}_{k_1(l_1+1)(m_1-1)} \hat{b}_{k_2(l_2+1)(m_2+1)}) \\
&\quad + \sqrt{(l_1 - m_1 + 1)(l_1 - m_1 + 2)(l_2 - m_2 + 1)(l_2 - m_2 + 2)} \hat{b}^\dagger_{k_1(l_1+1)(m_1-1)} \hat{b}^\dagger_{k_2 l_2 m_2} \hat{b}_{k_1 l_1 m_1} \hat{b}_{k_2(l_2+1)(m_2-1)} \\
&\quad + \sqrt{(l_1 + m_1 + 1)(l_1 + m_1 + 2)(l_2 + m_2 + 1)(l_2 + m_2 + 2)} \hat{b}^\dagger_{k_1(l_1+1)(m_1+1)} \hat{b}^\dagger_{k_2 l_2 m_2} \hat{b}_{k_1 l_1 m_1} \hat{b}_{k_2(l_2+1)(m_2+1)}].
\end{aligned} \tag{B1}$$

This expression only changes l and m one at a time, thus coupling (l, m) modes only to $(l \pm 1, m)$ or $(l \pm 1, m \pm 1)$. Together with angular momentum conservation, this allows for an efficient numerical implementation.

APPENDIX C: RELEVANT VARIABLES FOR THE TIME EVOLUTION OF GAUSSIAN STATES

Here we present the relevant variables required to perform the time evolution of the Gaussian state in the case of $n_0 = 0$. We find that even though the $\hat{\mathcal{H}}_{\mathrm{QLLP}}$ term defined in Appendix B is complicated, it simplifies due to the spherical symmetry of the problem, and we have

$$\eta_k = \frac{k^2}{2\mu_r}\phi_k + \frac{gk}{2\pi^2}\int_0^\Lambda dk' k' \phi_{k'} + \frac{k}{2M}\int_0^\Lambda k' 2(G_{kk'(l=1)}\phi_{k'} - F_{kk'(l=1)}\phi^*_{k'}) \tag{C1}$$

and

$$\mathcal{E}_{k_1 k_2 l} = \delta_{k_1 k_2}\frac{k_1^2}{2\mu_r} + \delta_{l,0}\frac{g k_1 k_2}{2\pi^2} + \frac{(l+1)k_i k_j}{(2l+1)M} G_{k_1 k_2 (l+1)} + \frac{l k_1 k_2}{(2l+1)M}(\delta_{l,1}\phi_{k_1}\phi^*_{k_2} + G_{k_1 k_2 (l-1)}), \tag{C2}$$

$$\Delta_{k_1 k_2 l} = -\frac{(l+1)k_1 k_2}{(2l+1)M} F_{k_1 k_2 (l+1)} - \frac{l k_1 k_2}{(2l+1)M}(\delta_{l,1}\phi_{k_1}\phi_{k_2} + F_{k_1 k_2 (l-1)}). \tag{C3}$$

The definitions of G and F are given in Eqs. (25) and (26).

[1] P. W. Anderson, More is different, Science **177**, 393 (1972).

[2] V. Efimov, Energy levels arising from resonant two-body forces in a three-body system, Phys. Lett. **33B**, 563 (1970).

[3] P. Naidon and S. Endo, Efimov physics: A review, Rep. Prog. Phys. **80**, 056001 (2017).

[4] T. Kraemer, M. Mark, P. Waldburger, J. G. Danzl, C. Chin, B. Engeser, A. D. Lange, K. Pilch, A. Jaakkola, H.-C. Nägerl, and R. Grimm, Evidence for Efimov quantum states in an ultracold gas of caesium atoms, Nature (London) **440**, 315 (2006).

[5] M. Kunitski, S. Zeller, J. Voigtsberger, A. Kalinin, L. P. H. Schmidt, M. Schöffler, A. Czasch, W. Schöllkopf, R. E. Grisenti, T. Jahnke, D. Blume, and R. Dörner, Observation of the Efimov state of the helium trimer, Science **348**, 551 (2015).

[6] P. Makotyn, C. E. Klauss, D. L. Goldberger, E. Cornell, and D. S. Jin, Universal dynamics of a degenerate unitary Bose gas, Nat. Phys. **10**, 116 (2014).

[7] S. Piatecki and W. Krauth, Efimov-driven phase transitions of the unitary Bose gas, Nat. Commun. **5**, 3503 (2014).

[8] U. Eismann, L. Khaykovich, S. Laurent, I. Ferrier-Barbut, B. S. Rem, A. T. Grier, M. Delehaye, F. Chevy, C. Salomon, L.-C. Ha, and C. Chin, Universal Loss Dynamics in a Unitary Bose Gas, Phys. Rev. X **6**, 021025 (2016).

[9] C. E. Klauss, X. Xie, C. Lopez-Abadia, J. P. D'Incao, Z. Hadzibabic, D. S. Jin, and E. A. Cornell, Observation of Efimov Molecules Created from a Resonantly Interacting Bose Gas, Phys. Rev. Lett. **119**, 143401 (2017).

[10] V. E. Colussi, J. P. Corson, and J. P. D'Incao, Dynamics of Three-Body Correlations in Quenched Unitary Bose Gases, Phys. Rev. Lett. **120**, 100401 (2018).

[11] C. Eigen, J. A. Glidden, R. Lopes, E. A. Cornell, R. P. Smith, and Z. Hadzibabic, Universal prethermal dynamics of Bose gases quenched to unitarity, Nature (London) **563**, 221 (2018).

[12] J. P. D'Incao, J. Wang, and V. E. Colussi, Efimov Physics in Quenched Unitary Bose Gases, Phys. Rev. Lett. **121**, 023401 (2018).

[13] V. E. Colussi, H. Kurkjian, M. Van Regemortel, S. Musolino, J. van de Kraats, M. Wouters, and S. J. J. M. F. Kokkelmans, Cumulant theory of the unitary Bose gas: Prethermal and Efimovian dynamics, Phys. Rev. A **102**, 063314 (2020).

[14] S. Musolino, H. Kurkjian, M. Van Regemortel, M. Wouters, S. J. J. M. F. Kokkelmans, and V. E. Colussi, Bose-Einstein Condensation of Efimovian Triples in the Unitary Bose Gas, Phys. Rev. Lett. **128**, 020401 (2022).

[15] J. Levinsen, M. M. Parish, and G. M. Bruun, Impurity in a Bose-Einstein Condensate and the Efimov Effect, Phys. Rev. Lett. **115**, 125302 (2015).

[16] Y. E. Shchadilova, R. Schmidt, F. Grusdt, and E. Demler, Quantum Dynamics of Ultracold Bose Polarons, Phys. Rev. Lett. **117**, 113002 (2016).

[17] S. M. Yoshida, S. Endo, J. Levinsen, and M. M. Parish, Universality of an Impurity in a Bose-Einstein Condensate, Phys. Rev. X **8**, 011024 (2018).

[18] N. B. Jørgensen, L. Wacker, K. T. Skalmstang, M. M. Parish, J. Levinsen, R. S. Christensen, G. M. Bruun, and J. J. Arlt, Observation of Attractive and Repulsive Polarons in a Bose-Einstein Condensate, Phys. Rev. Lett. **117**, 055302 (2016).

[19] M.-G. Hu, M. J. Van de Graaff, D. Kedar, J. P. Corson, E. A. Cornell, and D. S. Jin, Bose Polarons in the Strongly Interacting Regime, Phys. Rev. Lett. **117**, 055301 (2016).

[20] Z. Z. Yan, Y. Ni, C. Robens, and M. W. Zwierlein, Bose polarons near quantum criticality, Science **368**, 190 (2020).

[21] M. Cetina, M. Jag, R. S. Lous, I. Fritsche, J. T. Walraven, R. Grimm, J. Levinsen, M. M. Parish, R. Schmidt, M. Knap, and E. Demler, Ultrafast many-body interferometry of impurities coupled to a Fermi sea, Science **354**, 96 (2016).

[22] L. Landau, Über die Bewegung der Elektronen in Kristalgitter, Phys. Z. Sowjetunion **3**, 644 (1933).

[23] H. Fröhlich, Electrons in lattice fields, Adv. Phys. **3**, 325 (1954).

[24] S. P. Rath and R. Schmidt, Field-theoretical study of the Bose polaron, Phys. Rev. A **88**, 053632 (2013).

[25] A. Schirotzek, C.-H. Wu, A. Sommer, and M. W. Zwierlein, Observation of Fermi Polarons in a Tunable Fermi Liquid of Ultracold Atoms, Phys. Rev. Lett. **102**, 230402 (2009).

[26] F. Chevy, Universal phase diagram of a strongly interacting Fermi gas with unbalanced spin populations, Phys. Rev. A **74**, 063628 (2006).

[27] R. Combescot, A. Recati, C. Lobo, and F. Chevy, Normal State of Highly Polarized Fermi Gases: Simple Many-Body Approaches, Phys. Rev. Lett. **98**, 180402 (2007).

[28] L. A. Peña Ardila and S. Giorgini, Impurity in a Bose-Einstein condensate: Study of the attractive and repulsive branch using quantum Monte Carlo methods, Phys. Rev. A **92**, 033612 (2015).

[29] F. Grusdt, R. Schmidt, Y. E. Shchadilova, and E. Demler, Strong-coupling Bose polarons in a Bose-Einstein condensate, Phys. Rev. A **96**, 013607 (2017).

[30] N.-E. Guenther, R. Schmidt, G. M. Bruun, V. Gurarie, and P. Massignan, Mobile impurity in a Bose-Einstein condensate and the orthogonality catastrophe, Phys. Rev. A **103**, 013317 (2021).

[31] R. Schmidt and T. Enss, Self-stabilized Bose polarons, arXiv:2102.13616.

[32] P. Massignan, C. J. Pethick, and H. Smith, Static properties of positive ions in atomic Bose-Einstein condensates, Phys. Rev. A **71**, 023606 (2005).

[33] G. E. Astrakharchik and B. A. Malomed, Quantum versus mean-field collapse in a many-body system, Phys. Rev. A **92**, 043632 (2015).

[34] K. Chen, N. V. Prokof'ev, and B. V. Svistunov, Trapping collapse: Infinite number of repulsive bosons trapped by a generic short-range potential, Phys. Rev. A **98**, 041602(R) (2018).

[35] J. Levinsen, L. A. Peña Ardila, S. M. Yoshida, and M. M. Parish, Quantum Behavior of a Heavy Impurity Strongly Coupled to a Bose Gas, Phys. Rev. Lett. **127**, 033401 (2021).

[36] T. Shi, E. Demler, and J. I. Cirac, Variational study of fermionic and bosonic systems with non-Gaussian states: Theory and applications, Ann. Phys. (NY) **390**, 245 (2018).

[37] J. P. D'Incao and B. D. Esry, Mass dependence of ultracold three-body collision rates, Phys. Rev. A **73**, 030702(R) (2006).

[38] J. P. D'Incao and B. D. Esry, Enhancing the observability of the Efimov effect in ultracold atomic gas mixtures, Phys. Rev. A **73**, 030703(R) (2006).

[39] S.-K. Tung, K. Jiménez-García, J. Johansen, C. V. Parker, and C. Chin, Geometric Scaling of Efimov States in a ^{6}Li-^{133}Cs Mixture, Phys. Rev. Lett. **113**, 240402 (2014).

[40] R. Pires, J. Ulmanis, S. Häfner, M. Repp, A. Arias, E. D. Kuhnle, and M. Weidemüller, Observation of Efimov Resonances in a Mixture with Extreme Mass Imbalance, Phys. Rev. Lett. **112**, 250404 (2014).

[41] M. Sun and X. Cui, Enhancing the Efimov correlation in Bose polarons with large mass imbalance, Phys. Rev. A **96**, 022707 (2017).
[42] J. von Stecher, Five- and Six-Body Resonances Tied to an Efimov Trimer, Phys. Rev. Lett. **107**, 200402 (2011).
[43] F. Ferlaino, S. Knoop, M. Berninger, W. Harm, J. P. D'Incao, H.-C. Nägerl, and R. Grimm, Evidence for Universal Four-Body States Tied to an Efimov Trimer, Phys. Rev. Lett. **102**, 140401 (2009).
[44] A. Zenesini, B. Huang, M. Berninger, S. Besler, H.-C. Nägerl, F. Ferlaino, R. Grimm, C. H. Greene, and J. von Stecher, Resonant five-body recombination in an ultracold gas of bosonic atoms, New J. Phys. **15**, 043040 (2013).
[45] A. Christianen, J. I. Cirac, and R. Schmidt, Chemistry of a Light Impurity in a Bose-Einstein Condensate, Phys. Rev. Lett. **128**, 183401 (2022).
[46] T. D. Lee, F. E. Low, and D. Pines, The motion of slow electrons in a polar crystal, Phys. Rev. **90**, 297 (1953).
[47] R. Schmidt, From few- to many-body physics with ultracold atoms, Ph.D. thesis, Technische Universtät München, 2013.
[48] Y. E. Shchadilova, F. Grusdt, A. N. Rubtsov, and E. Demler, Polaronic mass renormalization of impurities in Bose-Einstein condensates: Correlated Gaussian-wave-function approach, Phys. Rev. A **93**, 043606 (2016).
[49] T. Shi, J. Pan, and S. Yi, Trapped Bose-Einstein condensates with attractive s-wave interaction, arXiv:1909.02432.
[50] T. Guaita, L. Hackl, T. Shi, C. Hubig, E. Demler, and J. I. Cirac, Gaussian time-dependent variational principle for the Bose-Hubbard model, Phys. Rev. B **100**, 094529 (2019).
[51] T. Shi, E. Demler, and J. I. Cirac, Variational Approach for Many-Body Systems at Finite Temperature, Phys. Rev. Lett. **125**, 180602 (2020).
[52] R. Jastrow, Many-body problem with strong forces, Phys. Rev. **98**, 1479 (1955).
[53] M. Drescher, M. Salmhofer, and T. Enss, Theory of a resonantly interacting impurity in a Bose-Einstein condensate, Phys. Rev. Research **2**, 032011(R) (2020).
[54] D. Blume, Few-boson system with a single impurity: Universal bound states tied to Efimov trimers, Phys. Rev. A **99**, 013613 (2019).
[55] M. Berninger, A. Zenesini, B. Huang, W. Harm, H.-C. Nägerl, F. Ferlaino, R. Grimm, P. S. Julienne, and J. M. Hutson, Universality of the Three-Body Parameter for Efimov States in Ultracold Cesium, Phys. Rev. Lett. **107**, 120401 (2011).
[56] R. Schmidt, S. P. Rath, and W. Zwerger, Efimov physics beyond universality, Eur. Phys. J. B **85**, 386 (2012).
[57] J. Wang, J. P. D'Incao, B. D. Esry, and C. H. Greene, Origin of the Three-Body Parameter Universality in Efimov Physics, Phys. Rev. Lett. **108**, 263001 (2012).
[58] P. Naidon, S. Endo, and M. Ueda, Physical origin of the universal three-body parameter in atomic Efimov physics, Phys. Rev. A **90**, 022106 (2014).
[59] J. Johansen, B. DeSalvo, K. Patel, and C. Chin, Testing universality of Efimov physics across broad and narrow Feshbach resonances, Nat. Phys. **13**, 731 (2017).
[60] R. Chapurin, X. Xie, M. J. Van de Graaff, J. S. Popowski, J. P. D'Incao, P. S. Julienne, J. Ye, and E. A. Cornell, Precision Test of the Limits to Universality in Few-Body Physics, Phys. Rev. Lett. **123**, 233402 (2019).
[61] X. Xie, M. J. Van de Graaff, R. Chapurin, M. D. Frye, J. M. Hutson, J. P. D'Incao, P. S. Julienne, J. Ye, and E. A. Cornell, Observation of Efimov Universality across a Nonuniversal Feshbach resonance in ^{39}K, Phys. Rev. Lett. **125**, 243401 (2020).
[62] E. Hiyama and M. Kamimura, Universality in Efimov-associated tetramers in ^{4}He, Phys. Rev. A **90**, 052514 (2014).
[63] L. Hackl, T. Guaita, T. Shi, J. Haegeman, E. Demler, and J. I. Cirac, Geometry of variational methods: Dynamics of closed quantum systems, SciPost Phys. **9**, 48 (2020).
[64] M. Drescher, M. Salmhofer, and T. Enss, Real-space dynamics of attractive and repulsive polarons in Bose-Einstein condensates, Phys. Rev. A **99**, 023601 (2019).
[65] R. A. W. Maier, M. Eisele, E. Tiemann, and C. Zimmermann, Efimov Resonance and Three-Body Parameter in a Lithium-Rubidium Mixture, Phys. Rev. Lett. **115**, 043201 (2015).
[66] B. Huang, I. Fritsche, R. S. Lous, C. Baroni, J. T. M. Walraven, E. Kirilov, and R. Grimm, Breathing mode of a Bose-Einstein condensate repulsively interacting with a fermionic reservoir, Phys. Rev. A **99**, 041602(R) (2019).
[67] C. J. Pethick and H. Smith, *Bose-Einstein Condensation in Dilute Gases* (Cambridge University Press, Cambridge, 2008).
[68] J. Ulmanis, S. Häfner, R. Pires, E. D. Kuhnle, Y. Wang, C. H. Greene, and M. Weidemüller, Heteronuclear Efimov Scenario with Positive Intraspecies Scattering Length, Phys. Rev. Lett. **117**, 153201 (2016).
[69] M. Eisele, R. A. W. Maier, and C. Zimmermann, Fast *In Situ* Observation of Atomic Feshbach Resonances by Photoassociative Ionization, Phys. Rev. Lett. **124**, 123401 (2020).
[70] M. Drescher, M. Salmhofer, and T. Enss, Quench Dynamics of the Ideal Bose Polaron at Zero and Nonzero Temperatures, Phys. Rev. A **103**, 033317 (2021).
[71] K. Seetharam, Y. Shchadilova, F. Grusdt, M. B. Zvonarev, and E. Demler, Dynamical Quantum Cherenkov Transition of Fast Impurities in Quantum Liquids, Phys. Rev. Lett. **127**, 185302 (2021).
[72] K. Seetharam, Y. Shchadilova, F. Grusdt, M. Zvonarev, and E. Demler, Quantum Cherenkov transition of finite momentum Bose polarons, arXiv:2109.12260.
[73] R. Schmidt and M. Lemeshko, Rotation of Quantum Impurities in the Presence of a Many-Body Environment, Phys. Rev. Lett. **114**, 203001 (2015).
[74] R. Schmidt and M. Lemeshko, Deformation of a Quantum Many-Particle System by a Rotating Impurity, Phys. Rev. X **6**, 011012 (2016).
[75] M. Lemeshko, Quasiparticle Approach to Molecules Interacting with Quantum Solvents, Phys. Rev. Lett. **118**, 095301 (2017).
[76] A. Camacho-Guardian, L. A. Peña Ardila, T. Pohl, and G. M. Bruun, Bipolarons in a Bose-Einstein Condensate, Phys. Rev. Lett. **121**, 013401 (2018).
[77] P. Naidon, Two impurities in a Bose-Einstein condensate: From Yukawa to Efimov attracted polarons, J. Phys. Soc. Jpn. **87**, 043002 (2018).
[78] G. Panochko and V. Pastukhov, Two- and three-body effective potentials between impurities in ideal BEC, J. Phys. A: Math. Theor. **54**, 085001 (2021).